

MODELING CELL GROWTH RESPONSE IN HORMONE REFRACTORY BREAST CANCER

A Thesis

Presented to the Faculty of the Graduate School
of Cornell University

in Partial Fulfillment of the Requirements for the Degree of
Master of Science

by

Joycelyn Faith Chan

August 2011

© 2011 Joycelyn Faith Chan
ALL RIGHTS RESERVED

ABSTRACT

Breast cancer is one of the prevailing cancers diagnosed among women today and the second leading cause of cancer death in women. Modeling breast cancer cell growth would be a useful tool in identifying therapeutically relevant targets while reducing the amount of spent resources. We have compiled a detailed signal transduction network incorporating epidermal growth factor receptor (EGFR) signaling and downstream components, such as PLC- γ , MAPK, PI3K/Akt, cell cycle signaling, transcription, and translation. Using mass-action kinetics, the model was formulated as a set of ordinary differential equations (ODEs). This resulted in more than 8,000 unknown parameters and more than 3,000 ODEs. Partitioning the original model into smaller sub-models and solving them individually may reduce run-time, while maintaining qualitatively similar results as the unpartitioned model. Experiments were performed on the MDA-MB-231 cell line to observe the effects of growth factor treatment on targets such as transcription factors and post-translationally modified proteins. Combination treatments of different growth factors resulted in negative synergy with respect to the chosen targets, which suggests interference between the different pathways involved in growth. This experimental data serves as a starting point to estimate an initial parameter set that can be used to obtain ensembles of parameters that emulate experimental results. In conclusion we have identified an approach to solving large-scale systems that can be used in conjunction with experimental data to predict novel therapeutic targets.

BIOGRAPHICAL SKETCH

Joycelyn Faith Chan was born in Pittsburgh, Pennsylvania. She graduated from Plum Senior High School in 2006 and like her two older brothers, continued her studies at Cornell University. In the Chemical and Biomolecular Engineering Department, she developed an interest in the field of biotechnology as an undergraduate researcher in Professor Jeffrey Varner's lab. She graduated with a Bachelor of Science degree in 2010. In her free time, Joycelyn enjoys playing piano, snowboarding, and soaking in the occasional ray of Ithaca sunshine.

To my parents, who have guided and supported me through all my endeavors.

ACKNOWLEDGEMENTS

I would first like to thank Professor Jeffrey Varner for giving me the opportunity to work in his lab for the past three years, as a graduate and an undergraduate student as well. As teacher and an advisor, he has done much to influence my academic growth. Next, I owe much of my development as a researcher to Ryan Tasseff, who, as a mentor and colleague, has always helped and guided me towards my goals, while encouraging me to think like a scientist. I would also like to thank fellow graduate students and friends Anirikh Chakrabarti, Joshua Lequieu, Anne Rocheleau, and Tom Mansell, for their support, advice, and valuable insight throughout this experience. Undergraduate researchers Anastasiya Dubrovina, Anita Gokhlay, Svetlana Ikonomova, Woojin Kim, Megan Altmire, and Kerianne Dobosz also made important contributions to this project.

TABLE OF CONTENTS

Biographical Sketch	iii
Dedication	iv
Acknowledgements	v
Table of Contents	vi
List of Tables	viii
List of Figures	ix
1 Introduction	1
1.1 Breast cancer development	2
1.1.1 HER2+/ER- breast cancer	2
2 Network Conception and Construction	10
2.1 ErbB signaling	10
2.2 Adaptor protein signaling	11
2.3 Mitogen-activated protein kinase (MAPK) pathway	13
2.3.1 Raf activation	13
2.3.2 Mitogen-activated protein kinase cascade	14
2.3.3 Feedback	14
2.4 PI3K pathway	15
2.5 PLC- γ pathway	16
2.6 Cell cycle	16
2.7 Transcription and translation	19
3 Materials and Methods	22
3.1 Experimental	22
3.1.1 Cell culture	22
3.1.2 Flow cytometry	23
3.1.3 Cell cycle analysis	25
3.1.4 Antibodies and growth factors	26
3.2 Computational	26
3.2.1 Formulation and solution of the model equations	26
3.2.2 Simulation protocol	28
3.2.3 Partitioning	29
3.2.4 Pareto Optimal Ensemble Techniques (POETs)	29
4 Results	32
4.1 Experimental	32
4.1.1 Growth factor treatment	33
4.1.2 Cell cycle analysis	34
4.2 Computational	36
4.2.1 Partitioning a smaller three-gene network	38
5 Discussion	45

6	Conclusions and Future Work	51
A	Supplemental Experimental Data	53
A.1	Flow cytometry results	53
A.2	Comparison of fluorescence intensity between unstained and stained samples	61
A.3	Statistical significance of combination treatments	65
B	Nomenclature table	66
	Bibliography	71

LIST OF TABLES

1.1	Cyclin-dependent kinases and corresponding cyclins. If a specific phase is not indicated, then that complex does not form. Also included are the cyclin-dependent kinase inhibitors that inhibit the function of Cdk2/4/6 (indicated with an "X").	8
2.1	Shc-independency/dependency of receptor dimer signaling. "Y" indicates that dimer can signal with respect to that pathway, and "N" indicates that it cannot. The ErbB3 homodimer is not included as it does not participate in adaptor protein signaling. .	12
2.2	Activation state of proteins/protein complexes involved in cell cycle regulation when phosphorylated.	17
2.3	Transcription factor activation/regulation.	21
A.1	<i>p</i> -values for phospho-ERK1/2. Intensity levels detected for phospho-ERK1/2 in each treated, antibody-stained sample were compared to intensity levels detected in untreated, antibody-stained samples with a two-sample Student's t-test.	54
A.2	<i>p</i> -values for phospho-Akt. Intensity levels detected for phospho-Akt in each treated, antibody-stained sample were compared to intensity levels detected in untreated, antibody-stained samples with a two-sample Student's t-test.	56
A.3	<i>p</i> -values for p53. Intensity levels detected for p53 in each treated, antibody-stained sample were compared to intensity levels detected in untreated, antibody-stained samples with a two-sample Student's t-test.	57
A.4	<i>p</i> -values for E2F1. Intensity levels detected for E2F1 in each treated, antibody-stained sample were compared to intensity levels detected in untreated, antibody-stained samples with a two-sample Student's t-test.	59
A.5	<i>p</i> -values for phospho-4E-BP1. Intensity levels detected for phospho-4E-BP1 in each treated, antibody-stained sample were compared to intensity levels detected in untreated, antibody-stained samples with a two-sample Student's t-test.	60
A.6	<i>p</i> -values from two-sample Student's t-test between unstained and stained samples. Values across all time points were grouped together and simultaneously analyzed in the t-test.	64
A.7	<i>p</i> -values from two-sample Student's t-test between the result due to a combination treatment ($\Delta_{EGF+NRG1}$) and the sum of a marker's response to just EGF and just NRG1 ($\Delta_{EGF} + \Delta_{NRG1}$). . .	65
B.1	Nomenclature reference index	66

LIST OF FIGURES

1.1	Epidermal growth factor signaling network. Extracellular ligands bind to membrane-bound receptors, which dimerize and autophosphorylate their intracellular kinase domains. Only the EGFR homodimer and EGFR-HER2 and HER2-ErbB3 heterodimers are shown as a simplification. Arrows indicate direction of signal flow. Flat arrowheads indicate inhibitory actions. A representative transcription factor is shown to demonstrate transcription. The membrane-bound state of certain species (e.g. PIP2, DAG) is not indicated.	4
2.1	Graphical map of transcription regulation. The transcription factors shown in the middle point to the genes they control. While most transcription factors initiate transcription of the respective genes, p53 (gene name: TP53) inhibits transcription of CHEK1. The faded genes without an indicated transcription factor are controlled by the transcription factors SRF, SP1, FOS-JUN, and/or MYC-MAX. These transcription factors are not included as regulators in the figure for simplicity as they induce transcription of most genes in the model.	20
4.1	Fluorescence intensity of phospho-ERK1/2. Flow cytometric analysis was performed on untreated and 1 nM EGF, 10 nM EGF, 1 nM NRG1, and 10 nM NRG1 treated cells. Complete treatment results can be found in Appendix A. Cells were fixed at 1 hour, 2 hours, and 24 hours before analysis. Intensity values were scaled as described in Materials and Methods. All samples were done in triplicate and standard error was plotted.	34
4.2	Fluorescence intensity of phospho-Akt. Flow cytometric analysis was performed on untreated, 1 nM EGF, 1 nM NRG1, and 1 nM EGF + 1 nM NRG1 treated cells. Cells were fixed at 1 hour and 2 hours before analysis. Intensity values were scaled as described in Materials and Methods. All samples were done in triplicate and standard error was plotted.	35
4.3	Fluorescence intensity of phospho-Akt. Flow cytometric analysis was performed on untreated, 10 nM EGF, 10 nM NRG1, and 10 nM EGF + 10 nM NRG1 treated cells. Cells were fixed at 1 hour and 2 hours before analysis. Intensity values were scaled as described in Materials and Methods. All samples were done in triplicate and standard error was plotted.	36

4.4	Fluorescence intensity of p53. Flow cytometric analysis was performed on untreated, 1 nM NRG1, and 1 nM EGF + 1 nM NRG1 treated cells. Complete treatment results can be found in Appendix A. Cells were fixed at 1 hour, 2 hours, and 24 hours before analysis. Intensity values were scaled as described in Materials and Methods. All samples were done in triplicate and standard error was plotted.	37
4.5	Fluorescence intensity of E2F1 after 24 hours of treatment. Flow cytometric analysis was performed on untreated, 1 nM EGF, 1 nM NRG1, 1 nM EGF + 1 nM NRG1, 10 nM EGF, 10 nM NRG1, and 10 nM EGF + 10 nM NRG1 treated cells. Complete treatment results can be found in Appendix A. Cells were fixed at 1 hour, 2 hours, and 24 hours before analysis. Intensity values were scaled as described in Materials and Methods. All samples were done in triplicate and standard error was plotted.	38
4.6	Fluorescence intensity of phospho-4E-BP1. Flow cytometric analysis was performed on untreated, 1 nM EGF, 10 nM EGF, 1 nM NRG1, and 10 nM NRG1 treated cells. Cells were fixed at 1 hour and 2 hours before analysis. Intensity values were scaled as described in Materials and Methods. All samples were done in triplicate and standard error was plotted.	39
4.7	Cell cycle distribution of untreated and treated cells. Cells were seeded and then starved for 24 hours before being treated with 1 nM EGF, 1 nM NRG1, and 1 nM EGF + 1 nM NRG1.	40
4.8	Cell cycle distribution of untreated and treated cells. Cells were seeded and then starved for 24 hours before being treated with 10 nM EGF, 10 nM NRG1, and 10 nM EGF + 10 nM NRG1.	40
4.9	Concentration profiles of protein 1 in the cytosol (P1_c) at sampled time points of 1, 100, 200, 800, and 1000 seconds. Both the unpartitioned model and two-partition model were run to steady state (data not shown). Both models were run for an additional 100 seconds before adding a perturbation in the form of one unit of ligand.	41
4.10	Concentration profiles of protein 1 in the cytosol (P1_c). After reaching steady state, a stimulus of ligand (one unit) was added 100 seconds later and the simulation was run for an additional 1000 seconds. While only changing the value of α , simulations were run using a two-partition model.	42
4.11	Simulated data from an unpartitioned 3-gene model. Data was scaled as in Equation 3.7.	43

4.12	Two-partition model simulations over parameter ensemble versus unpartitioned simulation. After reaching steady state, the simulations were run for an additional 1000 seconds before adding a stimulus of ligand. The response of protein 1 in the cytosol was recorded for the next 1000 seconds. Results from the ensemble were averaged and plotted with a margin of error (standard error \times 1.96), assuming a 95% confidence interval. . . .	44
5.1	Comparison between Δ fluorescence intensity from combination treatment and individual treatments of EGF and NRG1. Samples were treated with growth factor for 2 hours. The intensity detected in the control case (Section A.1 in Chapter A in Appendix) was subtracted from treated cases to obtain a delta of response (Δ). Δ_{EGF} (blue) and Δ_{NRG1} (green) were stacked and plotted next to $\Delta_{EGF+NRG1}$ (purple). The scale for phospho-Akt corresponds to the y-axis on the left and the scale for phospho-ERK1/2 corresponds to the y-axis on the right.	49
A.1	Response of phospho-ERK1/2 to low concentration growth factor treatments.	53
A.2	Response of phospho-ERK1/2 to high concentration growth factor treatments.	54
A.3	Response of phospho-Akt to low concentration growth factor treatments.	55
A.4	Response of phospho-Akt to high concentration growth factor treatments.	55
A.5	Response of p53 to low concentration growth factor treatments. .	56
A.6	Response of p53 to high concentration growth factor treatments.	57
A.7	Response of E2F1 to low concentration growth factor treatments.	58
A.8	Response of E2F1 to high concentration growth factor treatments.	58
A.9	Response of phospho-4E-BP1 to low concentration growth factor treatments.	59
A.10	Response of phospho-4E-BP1 to high concentration growth factor treatments.	60
A.11	Comparison of detected fluorescence for phospho-ERK1/2 between unstained and stained samples. Values across all time points were averaged and plotted with standard error. <i>p</i> -values listed in Table A.6.	61
A.12	Comparison of detected fluorescence for phospho-Akt between unstained and stained samples. Values across all time points were averaged and plotted with standard error. <i>p</i> -values listed in Table A.6.	62

A.13	Comparison of detected fluorescence for p53 between unstained and stained samples. Values across all time points were averaged and plotted with standard error. <i>p</i> -values listed in Table A.6.	62
A.14	Comparison of detected fluorescence for E2F1 between unstained and stained samples. Values across all time points were averaged and plotted with standard error. <i>p</i> -values listed in Table A.6.	63
A.15	Comparison of detected fluorescence for phospho-4E-BP1 between unstained and stained samples. Values across all time points were averaged and plotted with standard error. <i>p</i> -values listed in Table A.6.	64

CHAPTER 1

INTRODUCTION

Breast cancer is one of the prevailing cancers diagnosed among women today as well as the second leading cause of cancer death in women [43]. Current treatments include surgery, chemotherapy, radiation therapy, and targeted protein therapies [54]. None of these treatments are completely effective alone and are usually used in conjunction with one another. A particularly successful targeted therapy, trastuzumab (Herceptin[®], Genentech, Inc., member of the Roche Group), is a monoclonal antibody that targets the cell surface receptor HER2, which is commonly overexpressed in certain types of breast cancer [2]. The efficacy of this drug raises the question of whether other prominent proteins in breast cancer proliferation can be targeted to induce anti-proliferative effects. As the molecular players in breast cancer cells are innumerable, it would be difficult to test the effectiveness of targeting each one with bench top experiments. However, mathematical modeling of breast cancer cell growth would be a useful tool in identifying potential targets while reducing the amount of spent resources.

In this study, we aim to characterize hormone refractory growth by creating a network that encompasses multiple signaling pathways and feedback loops. Combining experimental and computational approaches will allow us to add another dimension of specificity by targeting breast cancer. In order to achieve this, we need to generate experimental data that is not only specific to breast cancer, but also applicable to computational model simulations/analysis.

1.1 Breast cancer development

The breast consists of a branching, ductal network embedded in fat. These ducts are made up of layers of epithelial cells, which continually proliferate, splitting and expanding the network [93]. When growth is unregulated, otherwise known as intraductal hyperplasia, epithelial cells fill the duct, leading to intraductal carcinoma *in situ* [55]. As growth continues, cells can break through the ductal basement membrane, a stage recognized as invasive carcinoma, and tumor formation can begin. Once this barrier is breached, cancerous cells can invade surrounding tissues or enter the bloodstream, leading to angiogenesis and metastasis.

1.1.1 HER2+/ER- breast cancer

The estrogen receptor is a nuclear receptor that binds to steroid hormones, more commonly called estrogens, the most dominant of which is estradiol. Upon estrogen-receptor binding, receptors dimerize and can then regulate gene expression by binding to estrogen response elements on the promoter regions of target genes [4]. However, estrogen-receptor negative (ER-) tumors do not depend on this type of signaling for growth. Rather, alternative pathways become the driving force behind uncontrolled cell proliferation. For example, the dysregulation of epidermal growth factor receptor (EGFR; see Table B.1 in Chapter B in Appendix for nomenclature index) signaling has been highly implicated in cancer. This receptor family, also known as ErbB, HER, or EGFR, consists of four trans-membrane receptor tyrosine kinases, which will be individually referred to as EGFR, HER2, ErbB3, and ErbB4. Three out of the four receptors bind

to extracellular ligands, but no ligands have been found to bind to HER2 [95]. Despite this, HER2 is the most potent oncoprotein in the family and overexpression of HER2 (HER2+) has been associated with worse prognosis [76]. Because HER2 does not depend on ligand binding for activation, it must dimerize with an activated form of itself or any other activated receptor. [27]. Upon dimerization, the receptor tyrosine kinases autophosphorylate themselves on the cytosolic tyrosine residues. These phosphotyrosine residues serve as docking sites for various intracellular proteins (Figure 1.1). Combinations of different protein complexes suspended at the cell membrane can lead towards different signaling pathways [95].

Ligand-receptor pairing

In the receptor family, EGFR and ErbB4 have the most binding partners. Well characterized ligands of ErbB1 include epidermal growth factor (EGF), amphiregulin (AREG), transforming growth factor alpha ($TGF\alpha$), betacellulin (BTC), heparin-binding growth factor (HBEGF), and epiregulin (EREG). ErbB4 also has the capacity to bind to BTC, HBEGF, and EREG, as well as the four members of the neuregulin family (NRG1, NRG2, NRG3, and NRG4). ErbB3 can bind to NRG1 and NRG2 [11]. However, ErbB3 lacks intrinsic kinase activity [29]. Similar to HER2, in order to activate the kinase domain, it must dimerize with another activated receptor, although HER2 is the preferred dimerization partner [95]. In fact, HER2 serves as the preferred heterodimerization partner out of all the ErbB receptors [27]. Due to its prominent role in upstream signaling, HER2 has been targeted in anti-cancer treatments. However, these treatments are not always effective, and interest has been shown in exploring

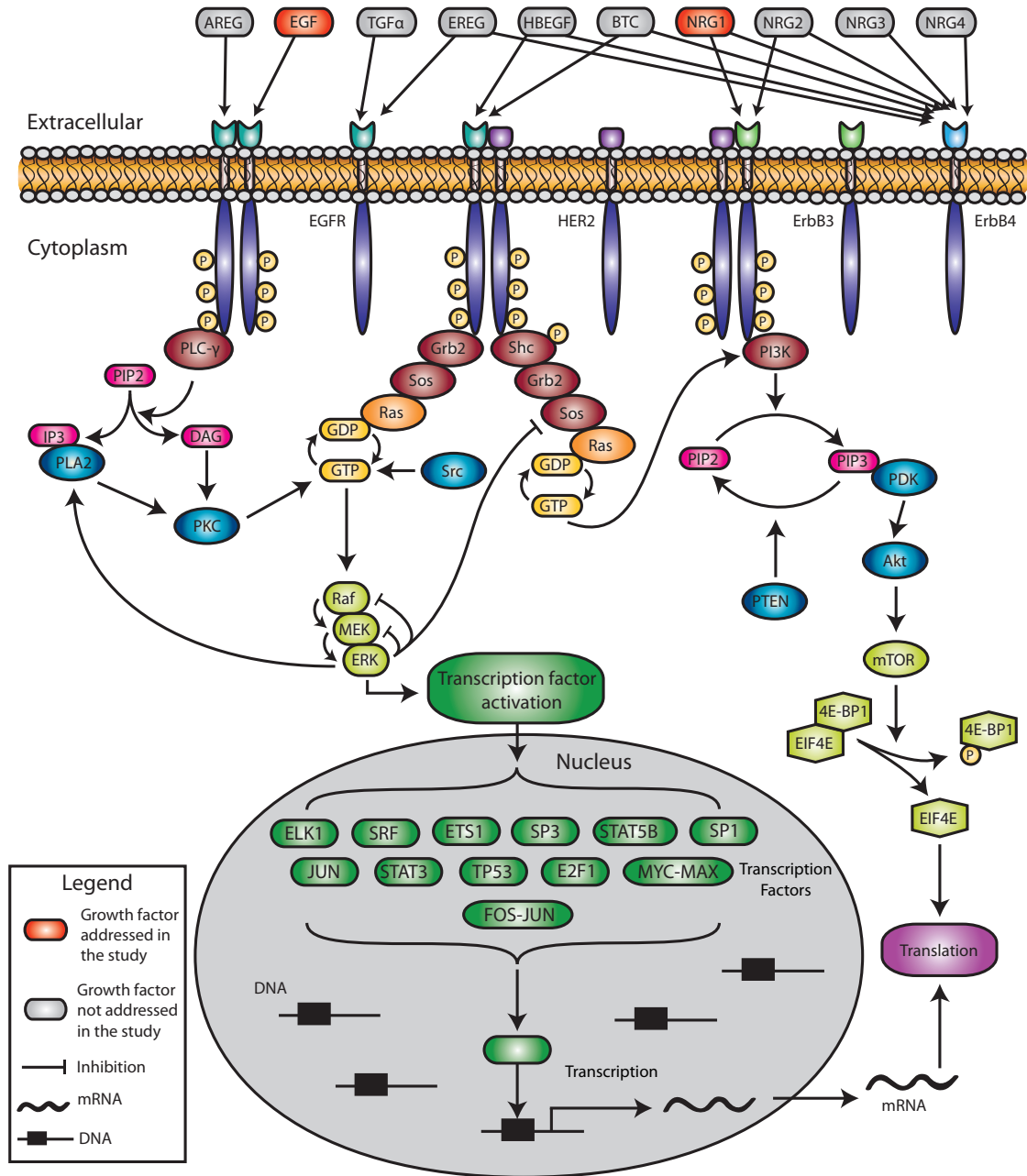


Figure 1.1: Epidermal growth factor signaling network. Extracellular ligands bind to membrane-bound receptors, which dimerize and autophosphorylate their intracellular kinase domains. Only the EGFR homodimer and EGFR-HER2 and HER2-ErbB3 heterodimers are shown as a simplification. Arrows indicate direction of signal flow. Flat arrowheads indicate inhibitory actions. A representative transcription factor is shown to demonstrate transcription. The membrane-bound state of certain species (e.g. PIP₂, DAG) is not indicated.

alternative targets [84].

Adaptor complexes

Once the tyrosine kinase domains of a receptor dimer are activated, adaptor proteins, such as Src homology 2 domain-containing protein (Shc), can bind to the domain and become tyrosine phosphorylated. Shc will then interact with growth factor receptor-bound protein 2 (Grb2), which subsequently binds Son of Sevenless homolog 1 (Sos), a rat sarcoma (Ras) guanine nucleotide exchange factor [70]. The Grb2-Sos complex can form independently of Shc as well for Grb2 can also be recruited directly to the phosphotyrosine domain [78]. Sos, suspended in the adaptor protein complex in close proximity to the membrane, can then exchange the guanosine diphosphate (GDP) bound to Ras for a guanosine triphosphate (GTP), activating Ras (Ras-GTP) [53].

Pathways

Upon activation, Ras can bind to Raf, the first kinase in the mitogen-activated protein kinase (MAPK) pathway, and by sequestering it to the membrane, lead to its activation. Activated Raf initiates a cascade of phosphorylation events by phosphorylating mitogen-activated protein kinase (MEK), which in turn phosphorylates extracellular-signal-regulated kinase (ERK). This activated form of ERK then translocates into the nucleus and activates a variety of transcription factors [80]. Although this pathway seems to be linear, positive and negative feedback loops keep the signaling cascade in control. Ras-GTP can also activate phosphoinositide 3-kinase (PI3K). PI3K phosphorylates phosphatidylinos-

itol 4,5-bisphosphate (PIP₂), a membrane phospholipid, to phosphatidylinositol 3,4,5-trisphosphate (PIP₃). Protein kinase B (Akt) preferentially binds PIP₃ and translocates to the membrane, where it is activated via phosphorylation by phosphoinositide-dependent kinase-1 (PDK). Activated Akt plays a role in cell proliferation and anti-apoptosis (cell survival) by regulating the function of an assortment of proteins. For example, Akt can inhibit the activity of cyclin dependent kinase inhibitors, which normally have anti-proliferative roles, and activate mammalian target of rapamycin (mTOR), which can stimulate mRNA translation into proteins [62].

Receptor tyrosine kinase domains can also directly phosphorylate phospholipase C gamma 2 (PLC). This activated form of PLC interacts with the cell membrane and cleaves PIP₂ into diacylglycerol (DAG) and inositol 1,4,5-triphosphate (IP₃). DAG remains at the membrane and serves to recruit protein kinase C for activation (PKC) [89], while IP₃ will bind to the IP₃ receptor on the endoplasmic reticulum, releasing stores of Ca²⁺ [71, 30]. This increase in calcium ion concentration will help sequester cytosolic phospholipase A₂ (PLA₂) to the membrane [64]. PLA₂ triggers the release of arachidonic acid, which stimulates PKC activation [82]. PKC is the kinase responsible for Raf activation [49].

Transcription and translation

Transcription is the process of converting genomic information, in the form of DNA (deoxyribonucleic acid), to mRNA (messenger ribonucleic acid), while translation is the process of interpreting mRNA into functional proteins. While there are multiple steps involved in gene transcription, the main step we have

focused on is binding of RNA polymerase I (RNAP) to the gene of interest. However, transcription factors or transcription factor complexes are needed to facilitate this binding. Once RNAP binds to a promoter region on DNA, it uses one of the helical strands to construct a complementary strand of mRNA. This mRNA undergoes additional processing to increase stability and is then exported out of the nucleus into the cytosol. For mRNA to be translated into protein, it must first bind an initiation complex composed of various initiation factors, each of which interacts with a different structural component of the mRNA. We have decided to represent this initiation factor complex with eukaryotic translation initiation factor 4E (EIF4E), the overexpression of which is often correlated to cancer. The 43S ribosome pre-initiation complex, composed of 40S small ribosomal subunit, methionyl tRNA, and additional initiation factors, joins the initiation complex. This eventually leads to 60S ribosomal subunit recruitment and translation is poised to begin at this point [83]. As full detail of the translational process is beyond the scope of this study, we have only included 40S and 60S binding, after which mRNA is committed to translation.

Cell cycle

The cell cycle, or the process of cell division, is composed of two main stages, mitosis, during which nuclear division occurs, and interphase, which is a period of normal cell growth. For modeling purposes, we have chosen to identify the signaling events that carry a cell through the three major phases of interphase, Gap 1 (G1), Synthesis (S), and Gap 2 (G2). During G1, the cell prepares for DNA replication, whereas DNA replication actually occurs in the S phase. After progressing through S phase, the cell prepares for mitosis during the G2

phase. Progression through these three phases is regulated by a group of kinases called cyclin-dependent kinases (CDK), which are activated at different points throughout the cycle. Although more CDKs have been identified, there are four that take part in cell cycle regulation - cyclin dependent kinase 1 (Cdk1), 2 (Cdk2), 4 (Cdk4) and 6 (Cdk6). As the name suggests, these enzymes are dependent on the presence, and binding, of proteins called cyclins, the levels of which periodically rise and fall according to the current phase. We will address four cyclins in this study - cyclin D (CycD), E (CycE), A (CycA) and B (CycB). Table 1.1 shows all possible cyclin-cyclin dependent kinase complex combinations included in the model as well as the corresponding phase in which they are active [68, 88]. As with most biological processes, cell cycle is tightly controlled, and cyclin-dependent kinase inhibitors, such as p21 and p27, can restrict CDK activity.

Table 1.1: Cyclin-dependent kinases and corresponding cyclins. If a specific phase is not indicated, then that complex does not form. Also included are the cyclin-dependent kinase inhibitors that inhibit the function of Cdk2/4/6 (indicated with an "X").

	Cdk1	Cdk2	Cdk4	Cdk6
CycA	G2/M transition	S	-	-
CycB	M	-	-	-
CycD	-	-	G1	G1
CycE	-	G1/S transition	-	-
p21 [†]	-	X	X	X
p27 [†]	-	X	X	X

[†] Cyclin dependent kinase inhibitors

An additional level of control comes in the form of Cdc25 phosphatases,

Cdc25A and Cdc25C, which are the enzymes responsible for activating CDKs. As kinases, the role of CDKs is to phosphorylate target proteins, such as the retinoblastoma protein (Rb). Rb is normally phosphorylated, at which point it is bound to the transcription factor E2F1, but upon further phosphorylation, it reaches a state of "hyperphosphorylation." At this point E2F1 is released from Rb, which is significant due to the ability of E2F1 to induce the transcription of many cell cycle genes. Other CDK targets include phosphatases that dephosphorylate Rb, transcription factors, and even Cdc25 phosphatases [68].

CHAPTER 2

NETWORK CONCEPTION AND CONSTRUCTION

While similar signaling networks have been described previously, this model in particular not only includes signaling from all four receptors and their corresponding ligands, but a simplified representation of cell cycle signaling as well. Transcription and translation reactions for all 72 distinct proteins present in the model have also been included. All reactions except for catalytic and degradation reactions are assumed to be reversible. All phosphorylation steps are accompanied by a separate dephosphorylation step, whether by a generic phosphatase (denoted by "Pase") or a specific regulator. Every species can degrade, while genes can be generated and degraded. General importers and exporters are used to transport proteins in and out of the nucleus and or cytosol.

2.1 ErbB signaling

Binding of extracellular ligands to ErbB receptors act as the driving force in the model. Reactions for this portion of the model were based on the system published by Schoeberl et al. [77], which only accounted for EGFR and one ligand. In this model, all four receptors as well as their corresponding ligands have been implemented. Each receptor, except for HER2, binds at least two different ligands. EGFR binds to EGF, AREG, TGF α , BTC, HBEGF, and EREG. ErbB4 binds to BTC, HBEGF, EREG, NRG1, NRG2, NRG3, and NRG4. ErbB3 can bind to NRG1 and NRG2 [11]. Though HER2 does not bind any ligands, it can dimerize with itself and autophosphorylate [74]. Each receptor can dimerize with another receptor [95]. This results in a total of ten possible receptor dimer combinations. The added complexity of ten different ligands results in more than

100 possible dimer formations. These dimers can then either degrade or become autophosphorylated. In accordance to the Schoeberl model, autophosphorylation is reversible. Also, there is no distinction as to which receptor or receptor tyrosine residue becomes phosphorylated. Rather, the dimer as a whole is denoted as phosphorylated. EGFR-containing dimers can also be phosphorylated by phosphorylated Src, a cellular tyrosine kinase (non-receptor) [51]. As stated before, ErbB3 homodimers lack intrinsic kinase activity [29], so while four different ErbB3 homodimers can form, they contribute to downstream signaling.

2.2 Adaptor protein signaling

The model published by Kholodenko et al. served as the basis for adaptor protein complex formation [47], which can be Shc-independent or Shc-dependent. In Shc-independent adaptor protein signaling, the activated dimer first binds Grb2. Sos then binds to the dimer-protein complex as well. At this point, the Grb2-Sos complex can either detach from the dimer and further dissociate into Grb2 and Sos, or remain bound to the dimer and "bind" Ras-GDP. After sequestering Ras-GDP to the dimer complex, Ras-GTP can then break off as a result.

In Shc-dependent adaptor protein signaling, the activated dimer binds Shc. Shc becomes phosphorylated and will either dissociate from the dimer complex in its activated form (and eventually deactivate) or remain bound to the dimer and bind to Grb2 and Sos one at a time, as in the Shc-independent pathway. After binding Sos, the entire adaptor protein complex, including phosphorylated Shc, can either detach from the dimer and further dissociate into its individual components, or bind Ras-GDP and release Ras-GTP [39, 7].

The availability of specific binding adaptor protein binding sites on each receptor determined whether certain dimers would participate in Shc-dependent or Shc-independent signaling, or even both (Table 2.1). ErbB4 can participate in Shc-dependent signaling, but the number of Grb2 binding sites on the tyrosine kinase domain is more dominant than that of Shc binding sites, so Shc-dependent signaling is not included for ErbB4. ErbB3-containing dimers can also bind and activate PI3K directly due to the abundance of PI3K binding sites on ErbB3 [78].

Table 2.1: Shc-independency/dependency of receptor dimer signaling. "Y" indicates that dimer can signal with respect to that pathway, and "N" indicates that it cannot. The ErbB3 homodimer is not included as it does not participate in adaptor protein signaling.

Receptor dimer combination	Shc-independent	Shc-dependent
EGFR-EGFR	Y	Y
EGFR-HER2	Y	Y
EGFR-ErbB3	Y	Y
EGFR-ErbB4	Y	Y
HER2-HER2	N	Y
HER2-ErbB3	N	Y
HER2-ErbB4	Y	Y
ErbB3-ErbB4	Y	N
ErbB4-ErbB4	Y	N

2.3 Mitogen-activated protein kinase (MAPK) pathway

Ras-GTP has multiple functions, one of which is to facilitate MAPK signaling by helping to activate Raf, the initiator of the protein phosphorylation events that characterize the MAPK pathway. As an additional form of control, we have included Ras GTPase activating protein (GAP) in the model, which can deactivate Ras by exchanging its GTP for GDP.

2.3.1 Raf activation

Raf must first be recruited to the plasma membrane by tyrosine 3-monooxygenase/tryptophan 5-monooxygenase activation protein (14-3-3) before undergoing phosphorylation. However, in order to bind 14-3-3, Raf needs to be phosphorylated at serine 259 (S259). Therefore, we distinguish phosphorylation at this site from general phosphorylation, which signifies activation. After 14-3-3 sequesters S259-phosphorylated Raf to the membrane, Raf can complex with Ras-GTP. Protein phosphatase 2 (PP2) can then release the Raf-Ras-GTP complex from 14-3-3 by dephosphorylating Raf at S259 [42]. The released Raf-Ras-GTP complex binds to activated PKC, and the resulting complex dissociates into the original components, only Raf is now phosphorylated, or activated [51].

The model also includes additional reactions to regulate Raf activation. For example, phosphorylated Akt can phosphorylate Raf at S259, but PP2 can negate this by dephosphorylating the site before 14-3-3 binding. Furthermore, the Raf-Ras-GTP complex may dissociate before binding PKC [42]. It is also possible for phosphorylated Src to bind the Raf-Ras-GTP complex and activate

Raf in a similar fashion as PKC [51].

2.3.2 Mitogen-activated protein kinase cascade

Phosphorylated Raf can then bind MEK, also known as MAPKK, and phosphorylate it. Phosphorylated Raf can also bind to phosphorylated MEK and phosphorylate it a second time to produce the fully activated version of MEK. Activated MEK is able to phosphorylate ERK, also known as MAPK, in a similar manner [77]. However, phosphatases can dephosphorylate Raf, MEK, or ERK at any point and hinder cascade flow, as seen in the Schoeberl model [77].

2.3.3 Feedback

We have incorporated feedback into the model as well. For example, activated ERK can phosphorylate Sos, which inhibits upstream adaptor protein signaling [7]. Activated ERK can also retrophosphorylate MEK [8] and Raf [91]. Although this implies that ERK is phosphorylating these upstream kinases, these events actually contribute to negative feedback, inhibiting cascade signaling. Therefore, in the model, this negative feedback is represented by dephosphorylation reactions as a simplification. An example of positive feedback present in the model would be how phosphorylated ERK can activate cytosolic phospholipase 2 (PLA2), which leads to production of more Ras-GTP [50], as explained in Section 2.5.

2.4 PI3K pathway

Aside from activation due to interactions with the ErbB3 tyrosine kinase domain, PI3K can also be activated by Ras-GTP [22]. Activated PI3K can then induce the conversion of PIP2 to PIP3. PIP3 will either revert to PIP2 through phosphatase and tensin homolog (PTEN) [34], or serve to recruit Akt and PDK to the membrane, where PDK will phosphorylate Akt. Activated Akt can then activate mTOR, the result of which will lead to translation and cell growth [62]. The tuberous sclerosis complex (TSC), composed of TSC1, also known as hamartin, and TSC2, also known as tuberin, plays an important role in the regulation of mTOR. The TSC1-TSC2 complex can catalyze the conversion of the GTPase Ras homolog enriched in brain (Rheb) from Rheb-GTP to Rheb-GDP. This downregulates mTOR activity as Rheb-GTP has the ability to activate mTOR. However, phosphorylated Akt can block this conversion by phosphorylating the TSC1-TSC2 complex directly, thereby inhibiting TSC1-TSC2 activity, or by phosphorylating TSC2 and preventing the formation of the TSC1-TSC2 complex [34].

Activated mTOR can either inactivate eukaryotic translation initiation factor 4E-binding protein 1 (4E-BP1) by phosphorylation and prevent it from binding eukaryotic translation initiation factor 4E (EIF4E), or release EIF4E by phosphorylating the 4E-BP1 component of the 4E-BP1-EIF4E complex [34]. Activated mTOR can also phosphorylate ribosomal protein S6 kinase (p70). Activated p70 can then activate the 40S ribosomal subunit (40S), allowing it to take part in translation.

2.5 PLC- γ pathway

Activated dimers, such as the ErbB1 homodimer, can also activate PLC [47]. Activated PLC can then cleave PIP2 into diacylglycerol (DAG) and inositol 1,4,5-triphosphate (IP3), both of which will lead to the activation of PKC. DAG has the ability to activate PKC directly, while as a simplification in the model, IP3 directly interacts with PLA2 to "activate" it. Another simplification is that "activated" PLA2 directly activates PKC. In addition to activating Raf, PKC also plays a role in loading Ras with GTP[94].

2.6 Cell cycle

Cyclins, cyclin dependent kinases (Cdk), and their respective complexes comprise an important regulatory aspect of the intricate biological process known as the cell cycle. However, phosphorylation states determine their activity. Some proteins/complexes are active when phosphorylated, and some are inactive. Table 2.2 describes cell cycle protein/complex activation states when phosphorylated.

Most of these complexes play some role in E2F1/retinoblastoma protein regulation. E2F1 is a transcription factor for various cell cycle genes, while the retinoblastoma protein (Rb) acts as a regulator for E2F1. Depending on its level of phosphorylation, Rb can sequester and inactivate E2F1 (low phosphorylation), or release E2F1 (high phosphorylation) [35]. In the model, Rb has three states - unphosphorylated (Rb), single phosphorylation (pRb) to represent hypophosphorylation, and dual phosphorylation (ppRb) to represent hyperphos-

Table 2.2: Activation state of proteins/protein complexes involved in cell cycle regulation when phosphorylated.

Protein/protein complex	Active or inactive
CycA-Cdk1	Inactive
CycA-Cdk2	Inactive
CycB-Cdk2	Inactive
CycD-Cdk4	Inactive
CycD-Cdk6	Inactive
CycE-Cdk2	Inactive
p21	Inactive
p27	Inactive
Cdc25A	Active
Cdc25C [†]	Active
Chk1 [‡]	Active
PP1	Inactive

[†]Inactive when dual phosphorylated

[‡]Dual phosphorylated

phorylation.

The complexes CycA-Cdk2, CycE-Cdk2, CycD-Cdk4, and CycD-Cdk6 have the ability to phosphorylate Rb directly, preventing E2F1 sequestration [17, 46, 48]. CycD-Cdk4/6 can also phosphorylate Rb while Rb is complexed with E2F1. The complex then dissociates into pRb and E2F1. However, pRb, still complexed with E2F1, can be phosphorylated again by CycE-Cdk2 and simultaneously release E2F1. The ppRb then can degrade. CycE-Cdk2 also has the ability to directly phosphorylate pRb to ppRb. Protein phosphatase 1 (PP1) can dephos-

phosphorylate pRb and ppRb [20] but CycA/E-Cdk2 and CycB-Cdk1 have the ability to phosphorylate, and thus deactivate, PP1 [52, 66].

The cyclin-CDK complexes also regulate other proteins aside from the E2F1-Rb complex. For example, CycA-Cdk2 can phosphorylate the transcription factor specificity protein 1 (Sp1), which is a transcription factor for the majority of the genes represented in the model [19]. CycB-Cdk1 phosphorylates and activates M-phase inducer phosphatase 3 (Cdc25C) [61, 37, 23]. It is then possible for Cdc25C to activate, by dephosphorylation, the CycB-Cdk1 complex, demonstrating a form of feedback [63, 38, 6]. Other activators of Cdc25C include polo-like kinase1 (PLK) [72, 67] and activated ERK [90]. Chk checkpoint homolog (Chk1) also phosphorylates Cdc25C, but with an inhibitory effect instead [9, 75]. In the model, this is indicated with a dual phosphorylation step. The double phosphorylated version of Cdc25C can then degrade.

When phosphorylated, another phosphatase, M-phase inducer phosphatase 1 (Cdc25A), activates, by dephosphorylation, CycA/E-Cdk2 [6, 68, 73]. Similar to the feedback exhibited by interactions between CycB-Cdk1 and Cdc25C, once activated, CycE-Cdk2 can phosphorylate and activate Cdc25A [38, 59]. Chk1, when dual phosphorylated, can inhibit Cdc25A activity in the same way that it inhibits Cdc25C [86, 21].

Cyclin dependent kinase inhibitors also have a regulatory role in cell cycle. We have incorporated two inhibitors, cdk inhibitor 1 (p21) and cdk inhibitor 1B (p27). p21 can bind directly to Cdk2/4/6, preventing them from complexing with cyclins [31], but the role of p27 is slightly more complex. For example, p27 binds to CycE-Cdk2 complexes to inhibit them [5]. However, the activated form of the CycE-Cdk2 complex can bind the CycE-Cdk2-p27 complex and phospho-

rylate p27, releasing the bound CycE-Cdk2 complex. Phosphorylated p27 will either become dephosphorylated or degraded [58, 81, 68]. CycE-Cdk2 can also be released from p27 by the CycD-Cdk4/6 complex, although p27 will not be phosphorylated as before [13]. Instead, p27 will simply dissociate from CycD-4/6. p27 can bind directly to CycD-Cdk4/6 complexes, but it will not inhibit activity. That is, CycD-Cdk4/6-p27 can carry out the same functions as CycD-Cdk4/6 with respect to the E2F1-Rb complex [18, 68]. Though normal functions of CycD-Cdk4/5 are not affected by p27, glycogen synthase kinase 3b (GSK) can phosphorylate CycD when complexed with p27, which marks the complex for degradation [12, 81]. Another p27 regulator, phosphorylated Src, can phosphorylate p27, restricting its inhibitory activity towards CycE-Cdk2 [15].

2.7 Transcription and translation

Basal transcription for every gene corresponding to the 72 proteins present in the model has been included. That is, it is only necessary for a gene to bind to RNA polymerase I (RNAP) and mRNA will be generated. mRNA will then be exported out of the nucleus, where it may be degraded or translated. We have included multiple transcription factors that control gene expression as well. Table 2.3 shows the various ways transcription factors are regulated in the model. Once transcription factors are activated, they are transported into the nucleus and can bind to the appropriate gene (along with RNAP) and initiate transcription. Figure 2.1 identifies which genes are controlled by which transcription factor.

Once mRNA is released from the nucleus, it can either degrade or bind with

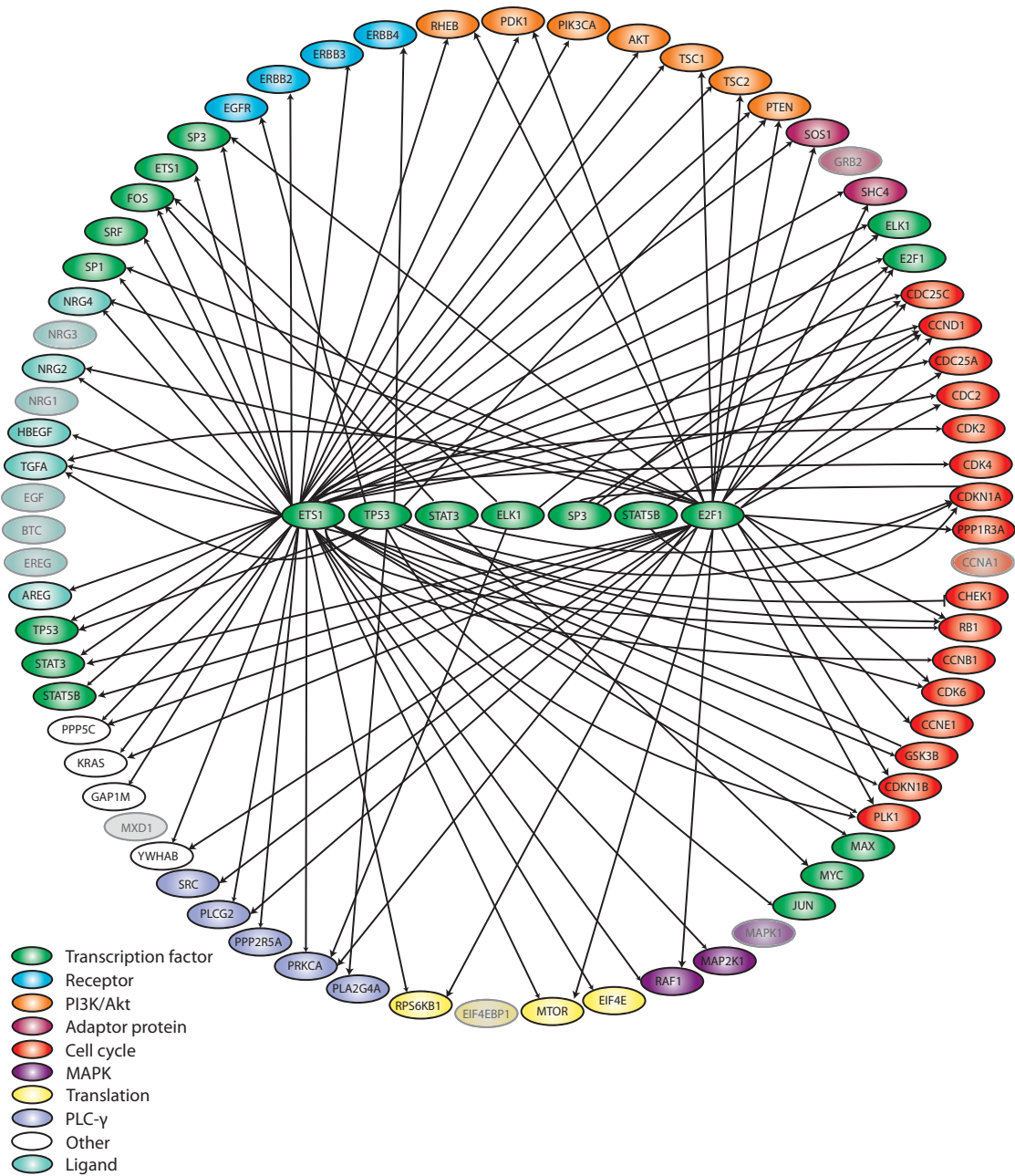


Figure 2.1: Graphical map of transcription regulation. The transcription factors shown in the middle point to the genes they control. While most transcription factors initiate transcription of the respective genes, p53 (gene name: TP53) inhibits transcription of CHEK1. The faded genes without an indicated transcription factor are controlled by the transcription factors SRF, SP1, FOS-JUN, and/or MYC-MAX. These transcription factors are not included as regulators in the figure for simplicity as they induce transcription of most genes in the model.

Table 2.3: Transcription factor activation/regulation.

Transcription factor	Regulation	Citation
Sp1	Phosphorylation by CycA-CDK2	[19]
	Phosphorylation by ERK	[56]
Fos-Jun complex	Phosphorylation by ERK	[57]
Myc-MAX complex	Phosphorylation by p-ERK	[28, 79]
MAX	Inhibition by MAD	[97, 14]
Myc	Degradation by GSK phosphorylation	[96, 79]
Srf	Phosphorylation by ERK	[3]
ETS1	Phosphorylation by ERK	[92]
E2F1	Inhibition by Rb	[81, 68]
STAT5B	Phosphorylation by ERK	[65]
ELK	Phosphorylation by ERK	[41]
STAT3	Phosphorylation by ERK	[16]
	Phosphorylation by Src	[69]

eukaryotic translation initiation factor 4E (EIF4E) and the ribosomal subunits, 40S and 60S. This complex then commits to translation and releases EIF4E. Next, the corresponding protein is released along with 40S, 60S, and the mRNA. This translation process is a simplified version of the system published previously by Nayak et al. [60].

CHAPTER 3

MATERIALS AND METHODS

3.1 Experimental

3.1.1 Cell culture

The human breast carcinoma cell line, MDA-MB-231, was received as a gift from the Claudia Fischbach-Teschl Lab (Cornell University, Ithaca, NY). Cells were cultured in Dulbecco's Modified Eagle's Medium (DMEM; Mediatech, Inc., Manassas, VA) supplemented with 10% fetal bovine serum (FBS; Lonza, Walkersville, MD) and 1% antibiotic-antimycotic (A/A) solution (10,000 units/mL penicillin G, 10 mg/mL streptomycin sulfate, and 25 μ g/mL amphotericin B). Cells were incubated in a humidified incubator kept at 37°C and 5% CO₂. To harvest cells, the media was first aspirated. The cell layer was then rinsed with phosphate buffered saline (PBS) to remove traces of serum. Cells were then incubated with 0.05% Trypsin/0.53 mM EDTA in Hank's Balanced Salt Solution (Mediatech, Inc., Manassas, VA) at 37°C until cells rounded up and detached from the surface. Regular culture media (10% FBS, 1% A/A) was added to re-suspend the cells. This solution was passed (1:2-5) in order to maintain stock, or centrifuged to reseed for experimental purposes.

In order to starve cells, cells were seeded in regular media overnight. The media was then aspirated and replaced by reduced serum media (RSM; DMEM supplemented with 0.1% fetal bovine serum, 1% antibiotic-antimycotic solution) for 24 hours in order to commence starvation.

Cells were grown in BD Falcon tissue culture flasks with vented caps (BD Biosciences, Bedford, MA) and Costar® tissue-culture treated 6-well plates (Corning, Inc., Lowell, MA; Cat No. 3516).

Cells were counted on a TC10™ automated cell counter (Bio-Rad, Hercules, CA) in a 50:50 ratio with Trypan Blue 0.4% solution (Lonza, Walkersville, MD).

To maintain frozen stock, cells were resuspended in freezing solution, consisting of DMEM, 10% FBS, and 5% dimethyl sulfoxide (DMSO) at a density of 2-3M. Samples were kept at -20°C overnight and then moved to a -80°C freezer for long-term storage.

3.1.2 Flow cytometry

Cells were seeded at 50% confluency (approximately 750,000 cells in 3 mL of media, or a density of 0.25M) in 6-well plates in 10% FBS media overnight. The next day, the media was replaced by RSM and cells were starved for 24 hours. After starvation, cells were treated with EGF, NRG1, or both to bring the final concentration of the respective growth factor to 1 nM or 10 nM. Treatments of different concentrations of growth factor were normalized to the same volume, while untreated samples were dosed with PBS. The flow cytometry protocol was adapted from the the protocol written by Cell Signaling Technolog (Danvers, MA). Cells were harvested and fixed for ten minutes at 37°C with 3% formaldehyde solution (3g/100mL PBS) assuming 1 mL fixing solution/1×10⁶ cells, at 1 hour, 2 hours, and 24 hours. Samples were then centrifuged and resuspended in PBS. Chilled 100% methanol, assuming 0.5 mL methanol/1×10⁶ cells, was added to bring the solution to 90% methanol. Samples were chilled on ice for 30 minutes.

After membrane permeabilization with methanol, samples were washed twice with incubation buffer. Incubation buffer was made as indicated by the flow cytometry protocol, consisting of 0.5 g of bovine serum albumin (BSA; Sigma-Aldrich Cat. No A2153) in 100 mL of PBS. Cells were then resuspended in 100 μ L of incubation buffer and blocked for ten minutes at room temperature. Cells were incubated with conjugated antibodies (1:50 ratio) for one hour in the dark at room temperature. Cells were washed twice with incubation buffer and resuspended in 400 mL of PBS for analysis on a BD LSR II flow cytometer using BD FACSDiva software at the Biomedical Sciences Flow Cytometry Core Laboratory at Cornell University located in Ithaca, NY. All samples were done in triplicate.

Data analysis

The mean fluorescence from each marker was recorded for each sample. Values for each marker were then scaled by dividing by the maximum intensity detected over all time points for that particular marker. That is, fluorescence values for p53 were divided by the maximum intensity detected for p53 over the entire experiment (regardless of time or treatment condition). Repeat samples were averaged and plotted with standard error. A two-sample Student's t-test was used to determine the statistical significance of treated sample measurements with respect to the untreated case (Section A.1 in Chapter A in Appendix).

Untreated samples were also prepared without antibody incubation and analyzed under the same conditions with flow cytometry. Intensity values for each marker were compiled across all time points and compared with corresponding control (with antibody incubation) data with a two-sample Student's t-test (Sec-

tion A.2 in Chapter A in Appendix).

3.1.3 Cell cycle analysis

Cells were seeded at 50% confluency (approximately 750,000 cells in 3 mL of media, or a density of 0.25M) in 6-well plates in 10% FBS media overnight. Media was changed to RSM and cells were starved for 24 hours. After starvation, cells were treated with EGF, NRG1, or both to bring the final concentration of the individual growth factor to 1 nM or 10 nM for 24 hours. Treatments of different concentrations of growth factor were normalized to the same volume, while untreated samples were dosed with PBS. After treatment, cells were harvested and washed with cold PBS twice. Cells were then resuspended in 400 μ L hypotonic staining solution, which consisted of PBS, 0.1% v/v Triton X-100 (Sigma-Aldrich, St. Louis, MO), 0.2 mg/mL RNase A (Sigma-Aldrich, St. Louis, MO), and 4% v/v propidium iodide (Sigma-Aldrich, St. Louis, MO) staining solution (propidium iodide dissolved in water at a concentration of 0.5 g/mL). Samples were incubated overnight at 4°C in the dark. Analysis was performed on a BD LSR II flow cytometer using BD FACSDiva software at the Biomedical Sciences Flow Cytometry Core Laboratory at Cornell University located in Ithaca, NY. All samples were done in triplicate.

The percentage of cells in G1, S, and G2/M phases were recorded for each sample. Percentages were averaged across repeats and plotted with standard error.

3.1.4 Antibodies and growth factors

Fluorophore-conjugated antibodies were used for flow cytometric analysis. Pre-conjugated monoclonal antibodies for p53 (Alexa Fluor[®] 488; Cat No. 2015), phosphorylated-p44/42 MAPK (Alexa Fluor[®] 647; Cat No. 4375), Ser473 phosphorylated-Akt (Alexa Fluor[®] 647; Cat No. 4075), and phosphorylated 4E-BP1 (Alexa Fluor[®] 488; Cat No. 2846) were obtained from Cell Signaling Technology (Danvers, MA). Monoclonal antibodies for E2F1 (Abcam, Cambridge, MA; Cat No. ab483) were conjugated using the Pacific Blue[™] monoclonal antibody labeling kit (Cat No. P30013) from Invitrogen (Carlsbad, CA).

Human recombinant Neuregulin-1 (NRG1; Cat No. 5218SF) was obtained from Cell Signaling Technology (Danvers, MA), and human recombinant epidermal growth factor (EGF; Cat No. PHG0311) was obtained from Invitrogen (Carlsbad, CA). For storage purposes, EGF and NRG1 were reconstituted in PBS (100 mg/mL) and aliquoted as needed for treatments.

3.2 Computational

3.2.1 Formulation and solution of the model equations

The breast model was formulated as a set of coupled Ordinary Differential Equations (ODEs):

$$\frac{d\mathbf{x}}{dt} = \mathbf{S} \cdot \mathbf{r}(\mathbf{x}, \mathbf{p}) \quad \mathbf{x}(t_o) = \mathbf{x}_o \quad (3.1)$$

The symbol \mathbf{S} denotes the stoichiometric matrix (3433×8178). The quantity \mathbf{x} denotes the protein and protein complex concentration (3433×1). The term

$\mathbf{r}(\mathbf{x}, \mathbf{p})$ denotes the vector of reaction rates (8178×1). Each row in \mathbf{S} described a species while each column described the stoichiometry of network interactions. Thus the (i, j) element of \mathbf{S} , denoted by σ_{ij} , described how protein i was involved in rate j . If $\sigma_{ij} < 0$, then protein i was consumed in r_j . Conversely, if $\sigma_{ij} > 0$, protein i was produced by r_j . Lastly, if $\sigma_{ij} = 0$, protein i was not involved in rate j .

We assumed mass-action kinetics for each interaction in the network. The rate expression for protein-protein interaction or catalytic reaction q :

$$\sum_{j \in \{\mathbf{R}_q\}} \sigma_{jq} x_j \rightarrow \sum_{p \in \{\mathbf{P}_q\}} \sigma_{pq} x_p \quad (3.2)$$

was given by:

$$r_q(\mathbf{x}, k_q) = k_q \prod_{j \in \{\mathbf{R}_q\}} x_j^{-\sigma_{jq}} \quad (3.3)$$

The set $\{\mathbf{R}_q\}$ denotes reactants for reaction q . The quantity $\{\mathbf{P}_q\}$ denotes the set of products for reaction q . The k_q term denotes the rate constant governing the q^{th} interaction. Lastly, σ_{jq} and σ_{pq} denote stoichiometric coefficients (elements of the matrix \mathbf{S}). We treated every interaction in the model as non-negative. All reversible interactions were split into two irreversible steps. The mass-action formulation, while expanding the dimension of the breast model, regularized the mathematical structure. The regular structure allowed automatic generation of the model equations. In addition, an analytical Jacobian (\mathbf{A}) and matrix of partial derivatives of the mass balances with respect to the model parameters (\mathbf{B}) were also generated. Mass-action kinetics also regularized the model parameters. Unknown model parameters were one of only three types, association, dissociation, or catalytic rate constants. Thus, although mass-action kinetics increased the number of parameters and species, they reduced the complexity of model analysis. In this study, we did not consider intracellular concentration

gradients. However, we accounted for membrane and cytosolic proteins by explicitly incorporating separate membrane and cytosolic protein species. We did consider a separate nuclear compartment and incorporated nuclear importers and exporters.

UNIVERSAL, an in-house code generation program (available for download at <http://code.google.com/p/universal-code-generator/>), was used to generate model code (mass balance equations, stoichiometric matrix, etc.), while SUNDIALS (SUite of Nonlinear and Differential/ALgebraic equation Solvers) [36] was used in Octave (www.octave.org) to solve the model equations.

3.2.2 Simulation protocol

An approximate steady-state was used as the starting point ($t = 0$ s) for all treatment simulations. Although no individual cell is likely to be at steady-state, we assumed that it was a reasonable approximation of the population average behavior of HER2+/ER- cells growing in the exponential phase. The steady-state was estimated numerically by repeatedly solving the model equations and estimating the difference between two subsequent time points:

$$\|\mathbf{x}(t + \Delta t) - \mathbf{x}(t)\|_2 \leq \varepsilon \quad (3.4)$$

The quantities $\mathbf{x}(t)$ and $\mathbf{x}(t + \Delta t)$ denote the simulated concentration vector at time t and $t + \Delta t$, respectively. The quantity $\|\cdot\|_2$ denotes the L_2 vector norm. In this study, $\Delta t = 100$ seconds of simulated time and $\varepsilon = 0.001$. Simulated time is not equivalent to the time-to-completion of a simulation (run-time).

3.2.3 Partitioning

To reduce run-time, a partitioning strategy was applied using the multi-way hypergraph partitioning algorithm published by the George Karypis Lab (Department of Computer Science and Engineering, University of Minnesota) [45]. The 8178 reactions of the original model were sorted into multiple "sub-models" in order to minimize the number of shared species between each sub-model, or partition. Mass balances were generated for each partition and solved independently. In order to preserve complete signal flow, after solving each time step, results from each partition were averaged together and used as the initial conditions across all partitions for the next time step:

$$IC_{t+t_s} = \frac{x_{1,t} + \dots + x_{N,t}}{N} \quad (3.5)$$

where IC represents initial conditions, x represents simulated concentrations at time t , and N represents the number of partitions.

3.2.4 Pareto Optimal Ensemble Techniques (POETs)

POETs is a multiobjective optimization strategy which integrates several local search strategies e.g., Simulated Annealing (SA) or Pattern Search (PS) with a Pareto-rank-based fitness assignment [85]. Denote a candidate parameter set at iteration $i + 1$ as \mathbf{k}_{i+1} . The squared error for \mathbf{k}_{i+1} for training set j was defined as:

$$E_j(\mathbf{k}) = \sum_{i=1}^{\tau_j} \left(\hat{\mathcal{M}}_{ij} - \hat{y}_{ij}(\mathbf{k}) \right)^2 \quad (3.6)$$

The symbol $\hat{\mathcal{M}}_{ij}$ denotes scaled experimental observations (from training set j) while the symbol \hat{y}_{ij} denotes the scaled simulation output (from training set j).

The quantity i denotes the sampled time-index and \mathcal{T}_j denotes the number of time points for experiment j . The training data was representative of experimental data, which is not always necessarily quantifiable. Suppose we have the intensity for species x at time $i = \{t_1, t_2, \dots, t_n\}$ in condition j . The scaled measurement would then be given by:

$$\hat{\mathcal{M}}_{ij} = \frac{\mathcal{M}_{ij} - \min_i \mathcal{M}_{ij}}{\max_i \mathcal{M}_{ij} - \min_i \mathcal{M}_{ij}} \quad (3.7)$$

Under this scaling, the lowest measurement equaled zero while the highest measurement equaled one. A similar scaling was defined for the simulation output.

We computed the Pareto rank of \mathbf{k}_{i+1} by comparing the simulation error at iteration $i+1$ against the simulation archive \mathbf{K}_i . We used the Fonseca and Fleming ranking scheme [24]:

$$\text{rank}(\mathbf{k}_{i+1} | \mathbf{K}_i) = p \quad (3.8)$$

where p denotes the number of parameter sets that dominate parameter set \mathbf{k}_{i+1} . Parameter sets on or near the optimal trade-off surface have small rank. Sets with increasing rank are progressively further away from the optimal trade-off surface. The parameter set \mathbf{k}_{i+1} was accepted or rejected by the SA with probability $\mathcal{P}(\mathbf{k}_{i+1})$:

$$\mathcal{P}(\mathbf{k}_{i+1}) \equiv \exp\{-\text{rank}(\mathbf{k}_{i+1} | \mathbf{K}_i) / T\} \quad (3.9)$$

where T is the computational annealing temperature. The initial temperature $T_o = n/\log(2)$, where n is user defined ($n = 4$ for this study). The final temperature was $T_f = 0.1$. The annealing temperature was discretized into 10 quanta between T_o and T_f and adjusted according to the schedule $T_k = \beta^k T_o$ where β was defined as:

$$\beta = \left(\frac{T_f}{T_o}\right)^{1/10} \quad (3.10)$$

The epoch-counter k was incremented after the addition of 100 members to the ensemble. Thus, as the ensemble grew, the likelihood of accepting parameter sets with a large Pareto rank decreased. We performed a local pattern-search every 5 steps to minimize the residual for the mean over the objective. The local pattern-search algorithm has been described previously [25, 87]. The parameter ensemble used in the simulation studies was generated from the low-rank parameter sets in \mathbf{K}_i .

CHAPTER 4

RESULTS

4.1 Experimental

After forming a hormone refractory based cancer growth model, we decided to generate experimental data specific to HER2+/ER- breast cancer. Because preliminary model simulations were based on growth factor stimulations, we chose to perform similar growth factor treatments on the MDA-MB-231 cell line. High (10 nM) and low (1 nM) dosages of EGF and NRG1, as well as combinations of the two, were administered to serum-starved cells. EGF was chosen due to its role in cell proliferation, while NRG1 was chosen for its specificity to the ErbB3 receptor, which is the only receptor that can activate the PI3K/Akt pathway. We chose phospho-ERK1/2, phospho-Akt, p53, E2F1, and phospho-4E-BP1 as our intracellular targets. Phospho-ERK1/2 is a common indicator of cell proliferation and phospho-Akt plays a role in cell survival and functions downstream of PI3K, which is activated by the ErbB3 receptor. E2F1 is a transcription factor for many cell cycle proteins, while p53 generally acts as a tumor suppressor. 4E-BP1 suppresses translation by sequestering EIF4E, but when 4E-BP1 becomes phosphorylated by mTOR, EIF4E is released. Therefore, we correlate the level of phospho-4E-BP1 to the level of translational processes in the cell. Fluorophore-conjugated antibodies for each marker were used and the resulting mean fluorescence was detected with flow cytometry. Analysis was performed at 1 hour, 2 hours, and 24 hours in order to capture short and long-term signaling.

4.1.1 Growth factor treatment

When cells were treated with 1 nM of EGF, phospho-ERK1/2 showed a significant increase after 2 hours, while with 10 nM, a significant change was observed within 1 hour (Figure 4.1). Differences in the levels of phospho-ERK1/2 between treated and control cases were only noticeable on a shorter time scale, as the levels of phospho-ERK1/2 from each case were comparable with the control by 24 hours. Interestingly, NRG1 treatments of 1 nM and 10 nM induced similar levels of phospho-ERK1/2 expression at 2 hours as the 1 nM treatment of EGF (Figure 4.1), which proves NRG1 has the ability to induce proliferation, but EGF is the dominant growth factor in that aspect. However, when cells were treated with both EGF and NRG1, the effects were not additive, in neither low nor high dosages (Figures A.1 and A.2 in Appendix A). This was also the case for phospho-Akt. While all treatments resulted in an increase of phospho-Akt at 1 and 2 hours, the magnitude of change did not vary significantly across treatment conditions, except for the 1 nM EGF treatment surprisingly (Figures 4.2 and 4.3). Because of the link between the ErbB3 receptor to the PI3K/Akt pathway, it would be expected that NRG1 would be a the dominant inducer of Akt activity. However, a low treatment of NRG1 did induce rapid degradation of p53. While in the control case p53 eventually degraded from 2 hours and onward, after being treated with NRG1 for 1 hour, the level of p53 was down to the final level of the control at 24 hours (Figure 4.4). This was also the case with the low combined dosage of NRG1 and EGF. In general, changes induced by high growth factor treatments were not significantly different from low growth factor treatments. For example, in the case of E2F1, increases were quantitatively similar at 24 hours across all treatment conditions (Figure 4.5). Also, with a 1 nM EGF treatment, a phospho-4E-BP1 signal was maintained from 1 to 2 hours,

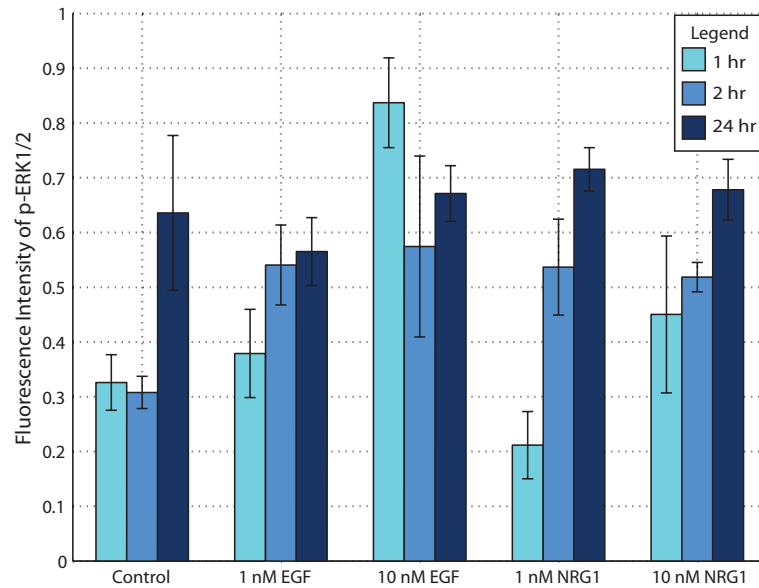


Figure 4.1: Fluorescence intensity of phospho-ERK1/2. Flow cytometric analysis was performed on untreated and 1 nM EGF, 10 nM EGF, 1 nM NRG1, and 10 nM NRG1 treated cells. Complete treatment results can be found in Appendix A. Cells were fixed at 1 hour, 2 hours, and 24 hours before analysis. Intensity values were scaled as described in Materials and Methods. All samples were done in triplicate and standard error was plotted.

while in other treatment cases, including the 10 nM EGF treatment, mean values decreased after 1 hour. With respect to the control, NRG1 seems to have more of an impact on phospho-4E-BP1 than EGF alone within 1 hour (Figure 4.6).

4.1.2 Cell cycle analysis

We performed a cell cycle analysis in order to verify that these signaling observations were in fact due to growth factor treatments and not a result of normal cell division. Cells were seeded and then starved for 24 hours before undergo-

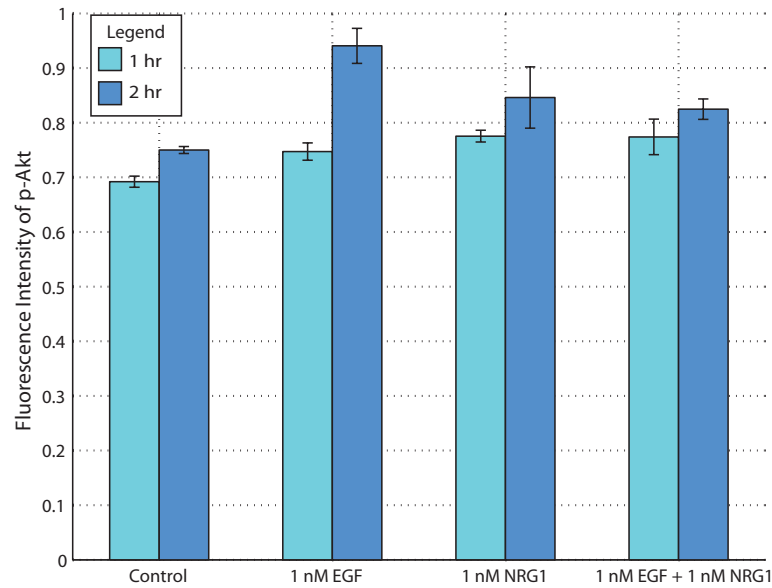


Figure 4.2: Fluorescence intensity of phospho-Akt. Flow cytometric analysis was performed on untreated, 1 nM EGF, 1 nM NRG1, and 1 nM EGF + 1 nM NRG1 treated cells. Cells were fixed at 1 hour and 2 hours before analysis. Intensity values were scaled as described in Materials and Methods. All samples were done in triplicate and standard error was plotted.

ing the same treatments (1 nM EGF, 10 nM EGF, 1 nM NRG1, 10 nM NRG1, 1 nM EGF + 1 nM NRG1, and 10 nM EGF + 10 nM NRG1). Cells were incubated in a hypotonic solution with propidium iodide to simultaneously permeabilize the membrane and stain DNA. The fluorescence intensity of propidium iodide was assumed to reflect the amount of DNA present in the cell. Samples were analyzed using flow cytometry after 24 hours of treatment. Figures 4.7 and 4.8 show the cell cycle distribution over all treatment conditions. With respect to the control, treatments do not seem to change the cell cycle distribution. After 24 hours of treatment, cells are dominantly in the G1 phase. This shows that for this particular cell line, the treatments that we chose are strong enough to induce growth signaling, but not enough to stimulate rapid cell growth, which

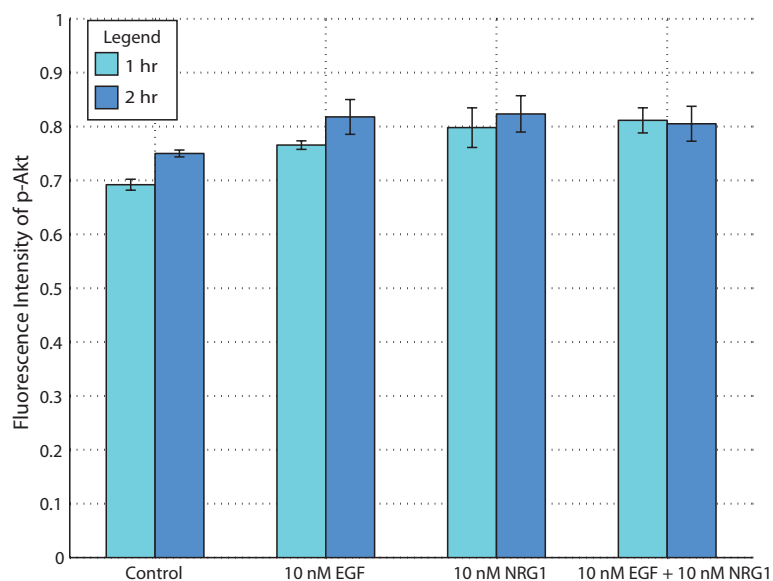


Figure 4.3: Fluorescence intensity of phospho-Akt. Flow cytometric analysis was performed on untreated, 10 nM EGF, 10 nM NRG1, and 10 nM EGF + 10 nM NRG1 treated cells. Cells were fixed at 1 hour and 2 hours before analysis. Intensity values were scaled as described in Materials and Methods. All samples were done in triplicate and standard error was plotted.

would result in a false positive in terms of markers such as phospho-ERK1/2.

4.2 Computational

Given current computational limitations, repetitively solving a model of 3433 ODEs soon becomes time-consuming and inconvenient for analysis. We investigated a method that would sort model reactions into smaller partitions that would hypothetically take less time to run. To test the partitioning strategy, a simplified model was used for analysis. This model, from now on referred to as the 3-gene model, is qualitatively similar to the breast cancer model in that it

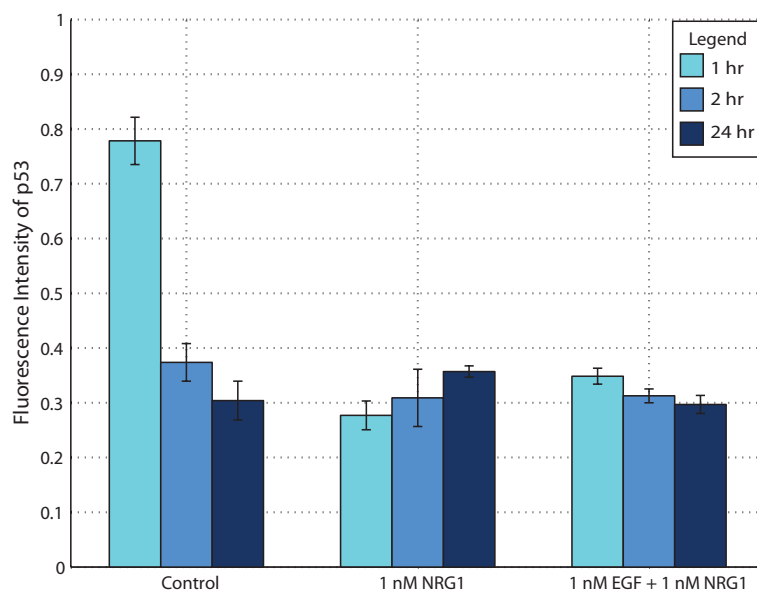


Figure 4.4: Fluorescence intensity of p53. Flow cytometric analysis was performed on untreated, 1 nM NRG1, and 1 nM EGF + 1 nM NRG1 treated cells. Complete treatment results can be found in Appendix A. Cells were fixed at 1 hour, 2 hours, and 24 hours before analysis. Intensity values were scaled as described in Materials and Methods. All samples were done in triplicate and standard error was plotted.

includes ligand-receptor binding that leads to activated transcription factor and the transcription and translation of three distinct genes. The smaller scale of the 3-gene model translates into faster run-time, making comparisons between partitioned model simulations and unpartitioned model simulations more feasible. When the 3-gene model was partitioned, the structural components of the resulting two partitions were intriguing. One partition contained upstream reactions, such as ligand-receptor binding and transcription factor activation, while the other partition contained mostly downstream transcription and translation reactions. It also should be noted that the model was sorted into equally sized partitions.

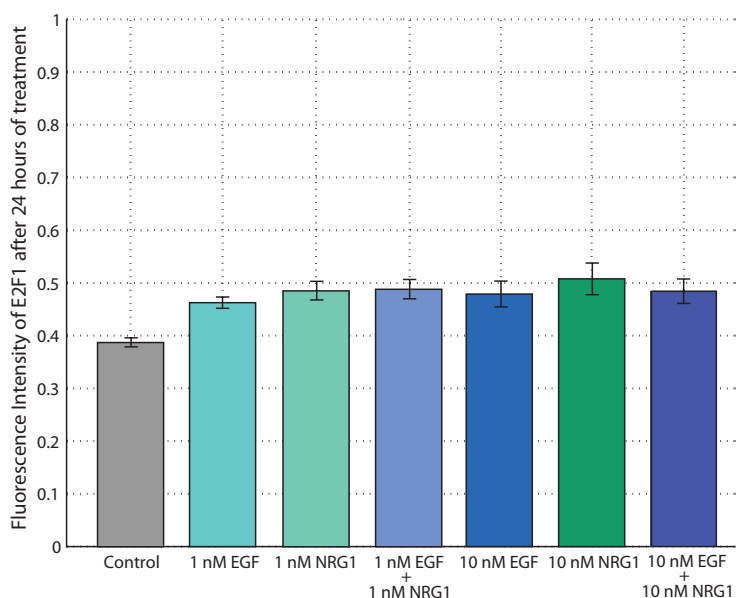


Figure 4.5: Fluorescence intensity of E2F1 after 24 hours of treatment. Flow cytometric analysis was performed on untreated, 1 nM EGF, 1 nM NRG1, 1 nM EGF + 1 nM NRG1, 10 nM EGF, 10 nM NRG1, and 10 nM EGF + 10 nM NRG1 treated cells. Complete treatment results can be found in Appendix A. Cells were fixed at 1 hour, 2 hours, and 24 hours before analysis. Intensity values were scaled as described in Materials and Methods. All samples were done in triplicate and standard error was plotted.

4.2.1 Partitioning a smaller three-gene network

First, it was necessary to determine if a partitioned model had the ability to reproduce qualitatively similar results as an unpartitioned model. A standard simulation was to run each model to steady state, and then introduce ligand after an additional 100 seconds. There should be an increase over time in protein 1 in the cytosol (P1_c), the production of which is directly correlated to ligand-receptor binding. Figure 4.9 shows the results of unpartitioned and partitioned model simulations. It can be seen that the two-partition model shows a qualitatively similar response with respect to P1_c. Also, using the same rate constant

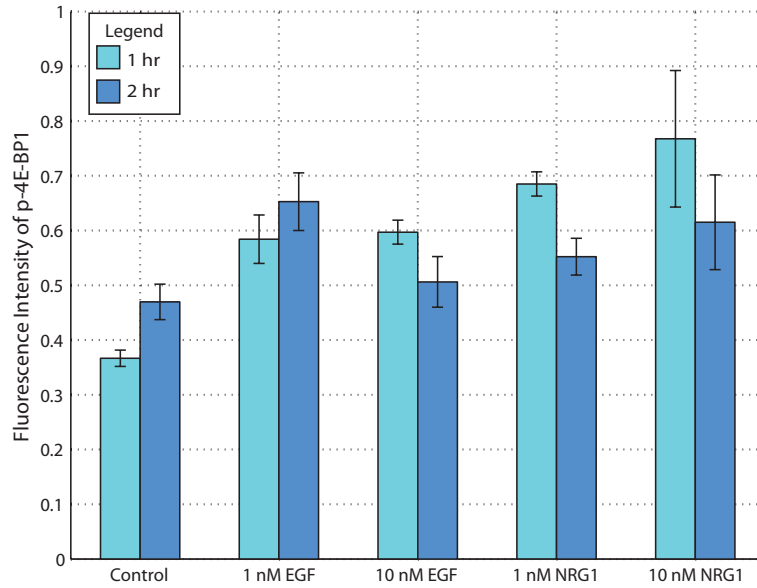


Figure 4.6: Fluorescence intensity of phospho-4E-BP1. Flow cytometric analysis was performed on untreated, 1 nM EGF, 10 nM EGF, 1 nM NRG1, and 10 nM NRG1 treated cells. Cells were fixed at 1 hour and 2 hours before analysis. Intensity values were scaled as described in Materials and Methods. All samples were done in triplicate and standard error was plotted.

parameters in each model, the scale of P1.c response from the two-partition model simulation is on par with the unpartitioned model simulation. However, at later time points the level of P1.c decreases, while in the unpartitioned model, the level of P1.c continues to gently increase. It is therefore concluded that the dynamics of the partitioned model differ from that of the unpartitioned model.

Partition Analysis

In order to identify the variability of results associated with partitioning, a partition constant, α , was defined. For example, in a two-partition system,

$$IC_{t+t_s} = \alpha x_{1,t} + (1 - \alpha)x_{2,t} \quad (4.1)$$

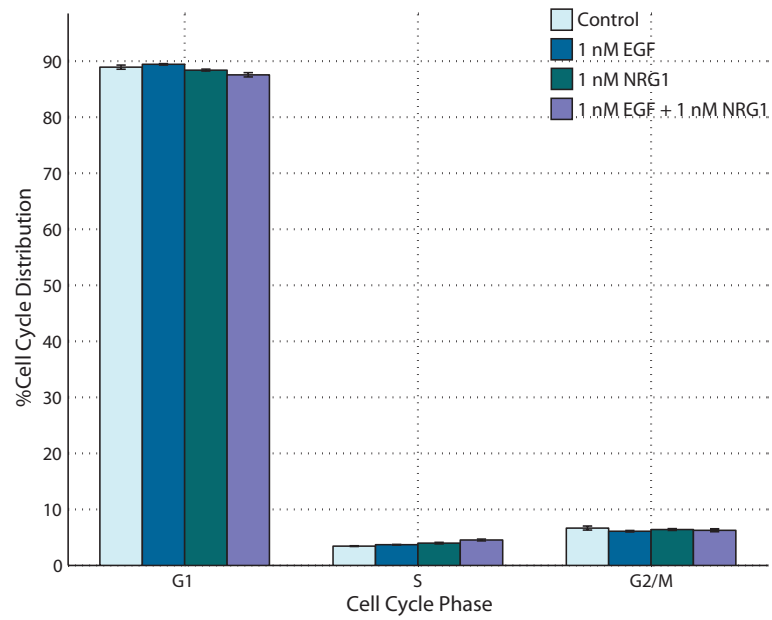


Figure 4.7: Cell cycle distribution of untreated and treated cells. Cells were seeded and then starved for 24 hours before being treated with 1 nM EGF, 1 nM NRG1, and 1 nM EGF + 1 nM NRG1.

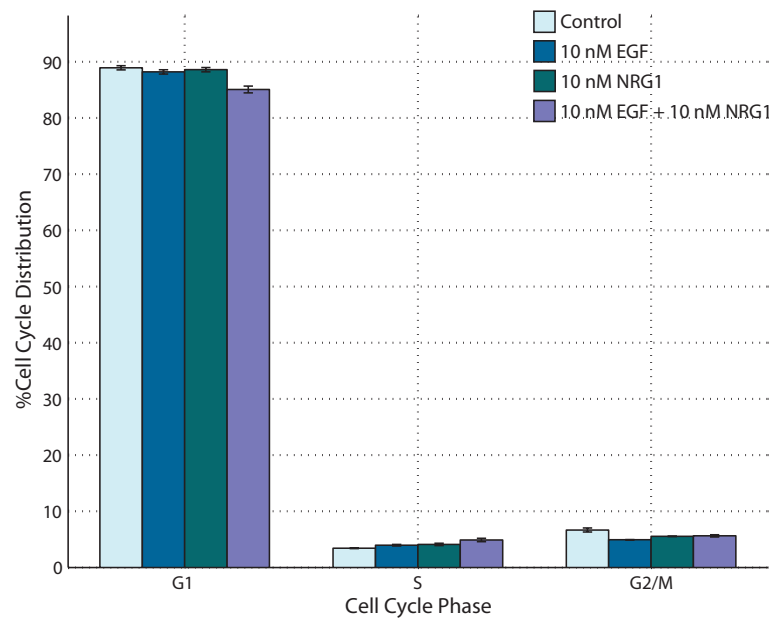


Figure 4.8: Cell cycle distribution of untreated and treated cells. Cells were seeded and then starved for 24 hours before being treated with 10 nM EGF, 10 nM NRG1, and 10 nM EGF + 10 nM NRG1.

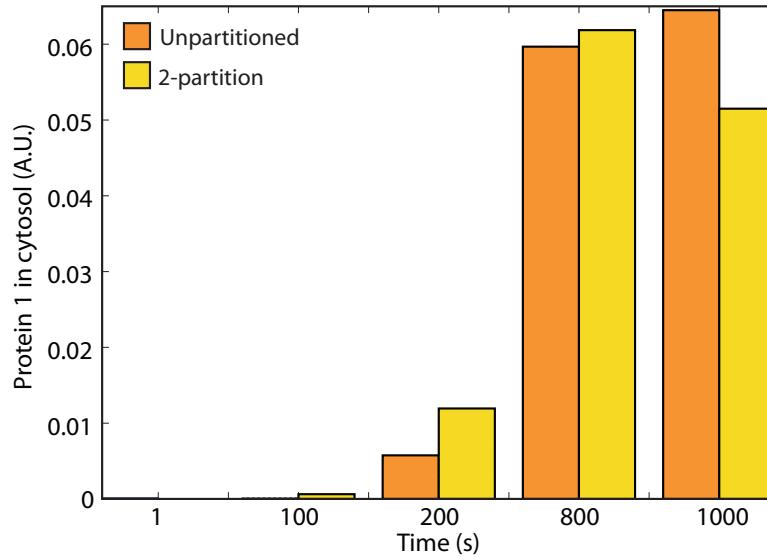


Figure 4.9: Concentration profiles of protein 1 in the cytosol (P1_c) at sampled time points of 1, 100, 200, 800, and 1000 seconds. Both the unpartitioned model and two-partition model were run to steady state (data not shown). Both models were run for an additional 100 seconds before adding a perturbation in the form of one unit of ligand.

Previously, when results were averaged, α equaled $1/N$. When α does not equal $1/N$, we are making the assumption that one partition's results should be favored when determining the initial conditions for the next time step. By running simulations with α set at different values between 0.1 and 0.9, we can observe a partitioned model's sensitivity to this new parameter that is not present in the unpartitioned model. Figure 4.10 shows the results from multiple two-partition simulations plotted alongside the results from an unpartitioned model simulation. It is clear that the value of α significantly affects the partitioned model's response to a stimulus. However, we believed there existed a parameter set that would reflect an unpartitioned model's response, qualitatively and dynamically regardless of the α value.

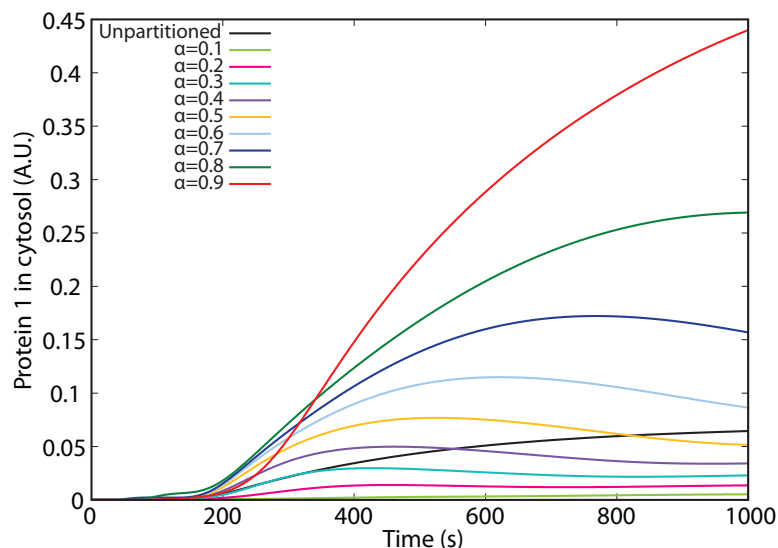


Figure 4.10: Concentration profiles of protein 1 in the cytosol (P1.c). After reaching steady state, a stimulus of ligand (one unit) was added 100 seconds later and the simulation was run for an additional 1000 seconds. While only changing the value of α , simulations were run using a two-partition model.

Estimation of a population of models using Pareto Optimal Ensemble Techniques (POETs)

POETs is typically used to obtain ensembles of model parameters that emulate various forms of experimental data (e.g. Western blots, ELISAs, immunoblots). Because the 3-gene network is not specific to any biological system, we “simulated” experimental data using an unpartitioned 3-gene model. We ran a stimulus simulation with the unpartitioned 3-gene model as done previously. This time, after reaching steady state, the model was run for an additional 1000 seconds before adding a unit of ligand. We make the assumption that bench-top experiments occur on a longer time-scale. The response was recorded for the next 1000 seconds. We chose four species to represent four distinct objectives - P1.c, protein 3 in the cytosol (P3.c), total transcription factor (TF), and total ac-

tivated transcription factor (aTF). The amounts of total transcription factor and total activated transcription factor were calculated by summing free TF/aTF and complexed TF/aTF values. We then chose four time points - 900, 1100, 1500 and 2000 time units. Only four markers and four time points were used in order to closely emulate a realistic set of experimental data. This data has been compiled in Figure 4.11. We generated 29 possible parameter sets and selected

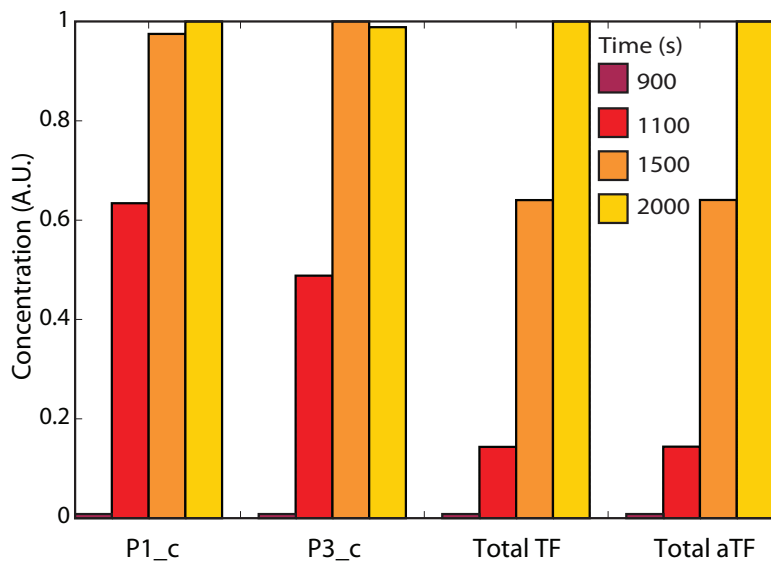


Figure 4.11: Simulated data from an unpartitioned 3-gene model. Data was scaled as in Equation 3.7.

those with low rank (1 or 0), resulting in a total of 18 sets for analysis. This ensemble was used to run simulations as before with the two-partition system. Results were scaled as in Equation 3.7. The average response of protein 1 in the cytosol across all 18 simulations is plotted alongside results from a simulation with an unpartitioned model in Figure 4.12. Despite a time lag early on, the response level of P1_c to the addition of ligand in a two-partition system continues to increase towards the end of the simulation, as opposed to preliminary simulations.

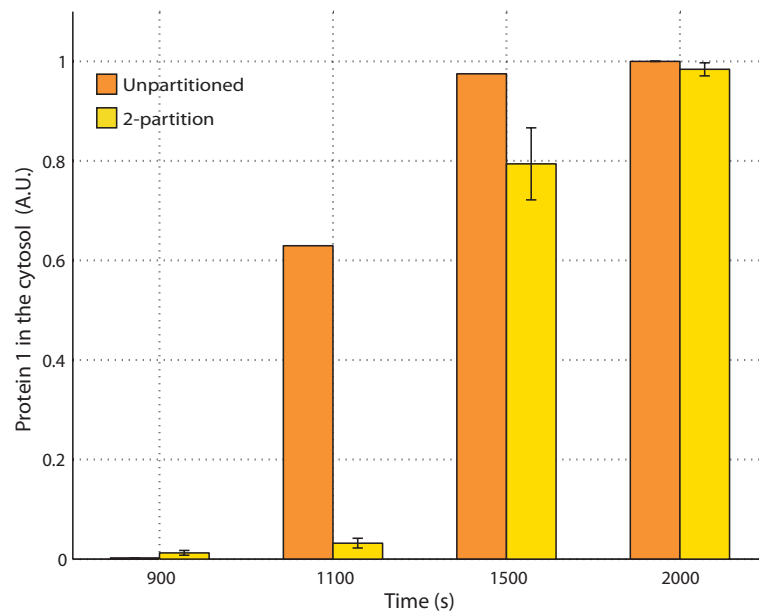


Figure 4.12: Two-partition model simulations over parameter ensemble versus unpartitioned simulation. After reaching steady state, the simulations were run for an additional 1000 seconds before adding a stimulus of ligand. The response of protein 1 in the cytosol was recorded for the next 1000 seconds. Results from the ensemble were averaged and plotted with a margin of error (standard error \times 1.96), assuming a 95% confidence interval.

CHAPTER 5

DISCUSSION

Using published experimental data, prior computational models of EGFR signaling, and protein interaction databases, we have compiled a comprehensive model of hormone-refractory cell growth. By incorporating multiple pathways and feedback loops, we hope to capture the intricacy and non-linearity of signaling driven by growth factors. Although our laboratory experiments were not designed to validate data from a particular set of computational simulations (or vice versa), from the network connectivity we hypothesized that growth factor stimulation would induce growth signaling. Likewise, we believed that treatments of multiple growth factors simultaneously and high concentration treatments would result in increased growth signaling, or at least indicate signal saturation. As EGF had specificity for EGFR, we believed that EGF would mainly activate the MAPK pathway, while NRG1, with specificity for ErbB3, would activate the PI3K/Akt pathway. However, flow cytometric analysis of EGF and/or NRG1 stimulated MDA-MB-231 cells for the selected markers (phospho-ERK1/2, phospho-Akt, E2F1, p53, and phospho-4E-BP1) did not completely correspond to this hypothesis.

While it was clear that a higher dose of EGF alone induced at 1 hour a statistically significant increase in phospho-ERK1/2 (Figure 4.1), a marker for cell proliferation, higher concentrations of growth factor did not consistently result in stronger or weaker signals. Also, the potency of signaling due to a 10 nM treatment of EGF was lost after 2 hours. At the 2 hour time point, phospho-ERK1/2 showed an increase with respect to the control, but the scaled mean fluorescence values across all treatment conditions did not vary significantly.

However, with regards to phospho-Akt, a 1 nM EGF treatment induced the highest overall (across all treatments and time points) phospho-Akt signal at 2 hours (Figure 4.2). Therefore, EGF is not necessarily limited to one particular pathway (MAPK) as we assumed and can upregulate PI3K/Akt as well. EGF may influence an increase in Ras-GTP (either through the MAPK or PLC- γ pathway) which has the ability to activate PI3K, and thus lead to Akt activation. Interestingly, a higher treatment of EGF (10 nM) did not lead to a linear increase in Akt activation. This gives reason to believe that phospho-ERK1/2 can inhibit Akt activation. One of the modes of negative feedback in the model consists of phospho-ERK phosphorylating Sos. Phosphorylated Sos is unable to associate with Grb2, the result of which restricts the production of Ras-GTP (Sos exchanges the GDP bound to Ras for GTP). This growth factor induced effect has also been demonstrated by Hayashi et al. [33]. Therefore, a high treatment of EGF must generate such a strong response of phospho-ERK1/2 that this negative feedback loop is triggered. The non-linearity of EGF signaling is further reflected in the response levels of phospho-4E-BP1. Despite a 10-fold difference in treatment concentration, the levels of phospho-4E-BP1 detected from a low and high EGF dose were comparable. This demonstrates that a low amount of EGF is enough to saturate the level of phospho-4E-BP1 at 1 hour and/or the higher treatment of EGF stimulates additional feedback loops that prevent a linear signal (e.g. Sos phosphorylation). Expression saturation was also reached in the case of E2F1. Regardless of treatment conditions, the increase (taking error into account) with respect to the untreated control at 24 hours was uniform.

NRG1 signaling is not exclusive to a particular pathway either. The fact that low and high treatments of NRG1 were able to stimulate a phospho-ERK1/2 signal as well as EGF treatments at 2 hours is not completely surprising, as the

HER2/ErbB3 heterodimer is thought to be a potent EGFR mitogenic signaling dimer when driven by neuregulin [1]. Nevertheless, other NRG1 treatment responses did correlate to the PI3K/Akt pathway. For example, a 1 nM treatment of NRG1 after 1 hour resulted in a sharp decrease in p53. This reflects the activation of Akt as Akt activates the Mdm2 (mouse double minute 2) p53 binding protein homolog [26]. Mdm2 then inhibits and contributes to the degradation of p53 [32]. This rapid degradation of p53 was also reflected in the simultaneous treatment of 1 nM EGF and 1 nM NRG1. It appears that EGF only slightly attenuated the response induced by NRG1. It is possible that phospho-ERK1/2 plays a role in stabilizing p53 in the MDA-MB-231 cell line [40]. If this is true, then it is plausible that EGF helps mitigate phospho-Akt-stimulated p53 degradation, knowing that phospho-ERK1/2 is a downstream target of EGF. This point is supported by the response of p53 to a 10 nM treatment of EGF (Figure A.6). There is no decrease in p53 and the average mean fluorescence is actually comparable to the control case. NRG1 was also able to stimulate an increase in phospho-4E-BP1, an indirect downstream target of the PI3K/Akt pathway. The difference in phospho-4E-BP1 levels between NRG1-treated and untreated cells is slightly greater than the difference between EGF-treated and untreated cells, which suggests that NRG1 has more of an ability to activate the PI3K/Akt pathway. This is not unreasonable, as ErbB3 signals directly to PI3K, while EGFR is likely to activate PI3K indirectly through Ras-GTP.

The non-linearity of growth factor signaling was also demonstrated in simultaneous treatments of EGF and NRG1. None of the responses of each marker to combination treatments were additive. To statistically compare the results from combination treatments to results from individual treatments, the respective control intensity value was subtracted from all treated samples. Deltas from

EGF-treated samples (Δ_{EGF}) and NRG1-treated (Δ_{NRG1}) samples were added together and this value was compared to the delta calculated from EGF+NRG1 treatments ($\Delta_{EGF+NRG1}$). A two-sample Student's t-test was used to determine whether differences were statistically significant (Table A.7). Although 1 nM treatments of EGF and NRG1 separately induced an increase in phospho-ERK1/2, this increase was not additive in the combination treatment (Figure A.1). It is possible that negative feedback loops are triggered at some threshold of phospho-ERK1/2 and that the MAPK and PI3K/Akt pathways counterbalance each other in order to check unregulated growth. A similar response was seen with phospho-Akt at 2 hours (Figure 5.1). The response of phospho-Akt to a 1 nM combination treatment did not reflect additive synergy. While the current version of our breast cancer model does not include any form of negative feedback with respect to Akt directly, there is evidence to believe that Akt activity can induce a downregulation in ErbB3 activity and expression [10]. ErbB3 inhibition would likely reduce the effect of NRG1 treatment on downstream signaling pathways. This theory is supported by the behavior of phospho-4E-BP1 in response to the same treatment at the same time point (not included in Figure 5.1; see Table A.7). However, the mechanism driving this feedback has yet to be revealed and requires further investigation.

While the level of detail included in the hormone-refractory cancer growth network is helpful in understanding different modes of regulation with respect to growth signaling, the resulting model becomes difficult to solve and simulation completion times become the rate-limiting step in terms of analysis. Therefore we have devised a partitioning strategy to essentially solve model equations in manageable "pieces" without sacrificing the original model connectivity. To test this strategy, we first applied it to a smaller 3-gene model. Initial

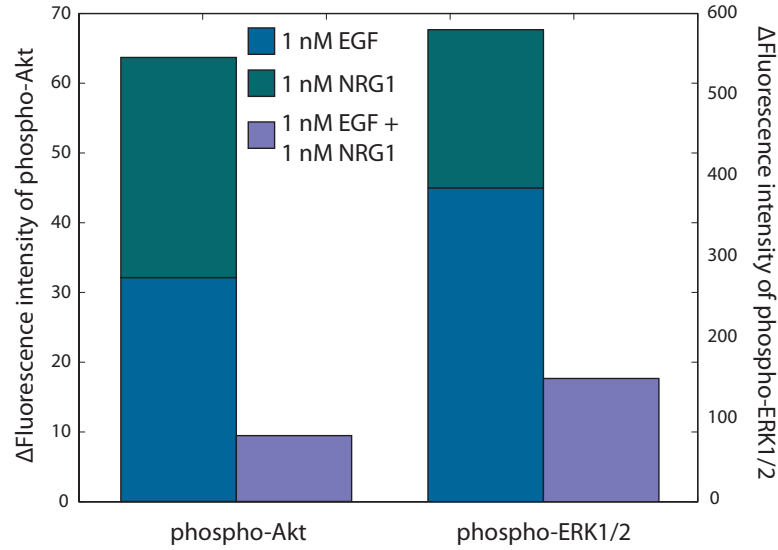


Figure 5.1: Comparison between Δ fluorescence intensity from combination treatment and individual treatments of EGF and NRG1. Samples were treated with growth factor for 2 hours. The intensity detected in the control case (Section A.1 in Chapter A in Appendix) was subtracted from treated cases to obtain a delta of response (Δ). Δ_{EGF} (blue) and Δ_{NRG1} (green) were stacked and plotted next to $\Delta_{EGF+NRG1}$ (purple). The scale for phospho-Akt corresponds to the y-axis on the left and the scale for phospho-ERK1/2 corresponds to the y-axis on the right.

simulation comparisons between an unpartitioned and a two-partition model showed that a partitioned model responded in a qualitatively similar fashion to addition of ligand. However, the partitioned model was accompanied by a new parameter, α , which determined how results from each partition were recombined after each time step. When the value of α was varied, the behavior of protein 1 in the cytosol's response to ligand varied as well. This is likely due to the structural differences in each partition. Performing a weighted average assumes that there is reason to believe one partition's results take precedence over the other. Because partitions are created in order to minimize the number of interacting species between each partition, while limiting overlaps as well, it is unlikely that one partition can arbitrarily be used to determine the other partition's

conditions. Each partition represents only a segment of the entire network, and it may be more accurate to identify an α value for each species. However, in a larger model with 3433 species, this quickly complicates an already-complex system. Therefore, for the purpose of POETs, an α value of 0.75 was chosen to give precedence to the partition with upstream signaling events. After obtaining 18 low rank parameter sets, it was observed that the behavior of P1.c, in comparison to original partitioned model simulations, changed in response to ligand. Instead of a transient signal, the level of P1.c continually rises, as in the unpartitioned model simulation. We determined that it was possible to use POETs to identify an ensemble of parameters that would allow a partitioned model to behave like an unpartitioned model. Running POETs for a longer period of time to generate more parameter sets would provide a more thorough analysis, but with this preliminary study we have revealed a tool to solve large-scale systems.

CHAPTER 6

CONCLUSIONS AND FUTURE WORK

We have developed a unique, detailed, hormone refractory cancer growth model comprised of ligand-receptor signaling, cell proliferation/survival pathways, cell cycle, and transcription/translation of genes. The detail and scope of the network translated into 8178 reactions and 3433 ODEs. To identify inherent characteristics of HER2+/ER- breast cancer signaling, we used the MDA-MB-231 cell line to perform growth factor experiments. By selecting the targets phospho-ERK1/2, phospho-Akt, p53, E2F1, and phospho-4E-BP1, we aimed to observe the activation of different downstream signaling pathways induced by EGF and NRG1. We observed that growth factor treatment upregulated these pathways, but certain treatments caused downregulation as well. This unexpected observation suggests that these signaling pathways are not linear and that they intersect at certain points in order to maintain balance in terms of growth. While this data may not necessarily be able to describe 8178 parameters, it provides a starting point towards characterizing HER2+/ER- breast cancer cell growth. In addition, now that we have been able to employ a technique with reasonable throughput to generate experimental growth factor treatment data, we can utilize the same method to observe the effects of these growth factors on different sections of the network, such as cyclin expression. Putting more focus on cell cycle protein expression would further elucidate the link between the current incorporated pathways and cell division. This data in conjunction with the data collected in this study could serve to better characterize the model, which would undergo further analysis to obtain ensembles of parameter sets that emulate the experimental results. Also, our partitioning strategy remains to be applied to the larger model, but this preliminary, develop-

mental step is critical in terms of approaching large-scale systems. In this epidermal growth factor signaling network, we have modeled only a few pathways involved in cell proliferation, but biologically, there is no shortage of additional pathways/regulators that have just as an important role. For example, Jones et al. performed an extensive analysis of the dysregulated pathways that contribute to pancreatic cancer [44]. Out of a population of pancreatic tumors, they identified 12 core signaling pathways that were consistently altered. However, the specific genetic alterations involved in each pathway varied between individual tumors. This demonstrates and emphasizes the fact that "cancer" cannot be studied by narrowly examining a subset of signaling pathways. Rather, the system that these pathways comprise must be considered in its entirety. Creating an expansive interaction network that integrates these pathways together would provide a better understanding of the interplay involved in growth dysregulation. However, this task is in no way insignificant computationally and requires the investigation of alternative methods other than brute force in terms of solving model equations. Our partitioning tool not only gives us the option to expand the network and elaborate on the current connectivity, but it also serves as the catalyst to propel this investigation forward. This strategy may not be the final solution, but only time and effort will reveal the optimal approach, bringing us one step closer to identifying novel therapeutic targets and assisting patients with unmet medical needs.

APPENDIX A

SUPPLEMENTAL EXPERIMENTAL DATA

A.1 Flow cytometry results

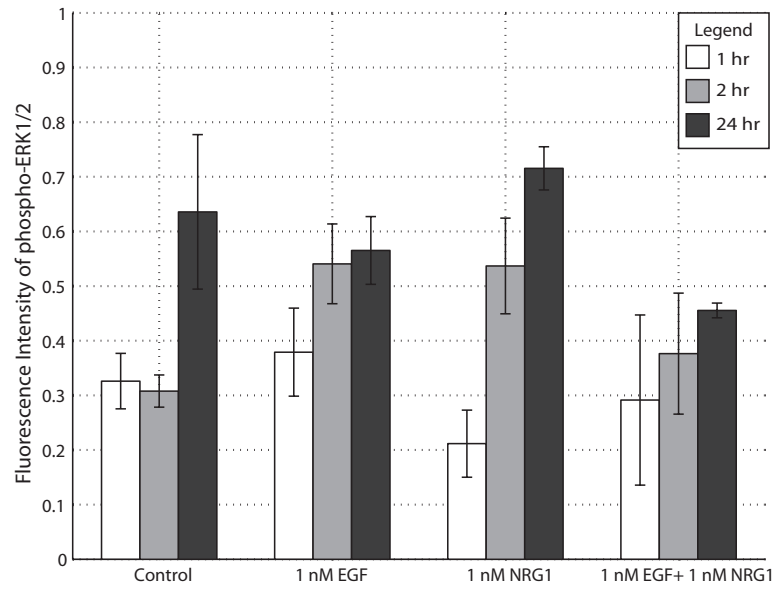


Figure A.1: Response of phospho-ERK1/2 to low concentration growth factor treatments.

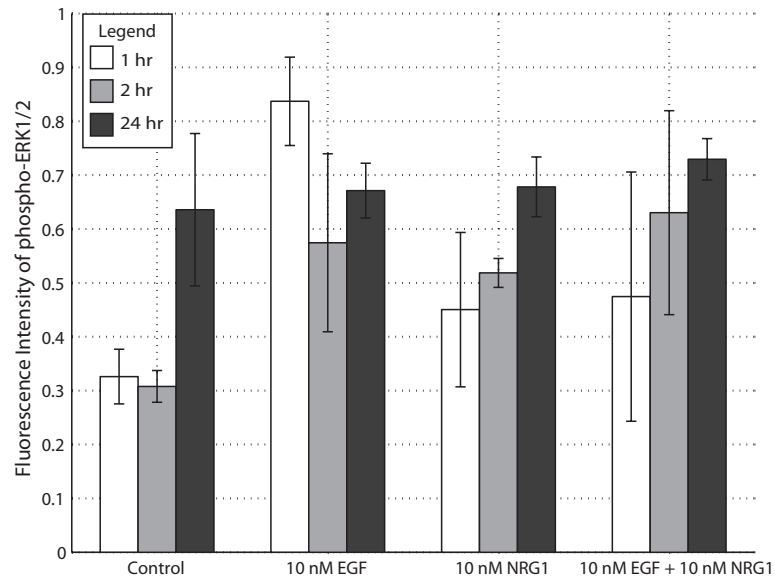


Figure A.2: Response of phospho-ERK1/2 to high concentration growth factor treatments.

Table A.1: p -values for phospho-ERK1/2. Intensity levels detected for phospho-ERK1/2 in each treated, antibody-stained sample were compared to intensity levels detected in untreated, antibody-stained samples with a two-sample Student's t -test.

Treatment	p-values for phospho-ERK1/2		
	1 hour	2 hours	24 hours
1 nM EGF	0.612	0.069	0.680
1 nM NRG1	0.226	0.108	0.634
1 nM EGF + 1 nM NRG1	0.849	0.604	0.329
10 nM EGF	0.010	0.245	0.831
10 nM NRG1	0.484	0.006	0.800
10 nM EGF + 10 nM NRG1	0.589	0.228	0.580

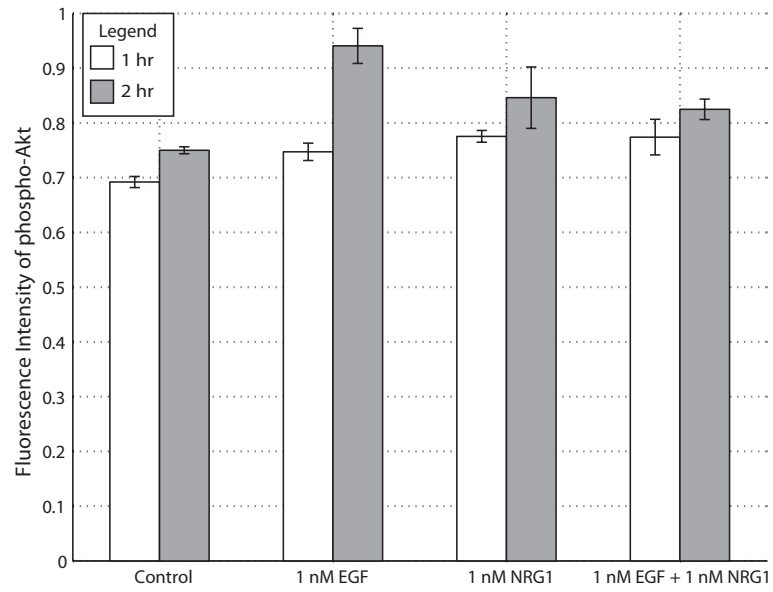


Figure A.3: Response of phospho-Akt to low concentration growth factor treatments.

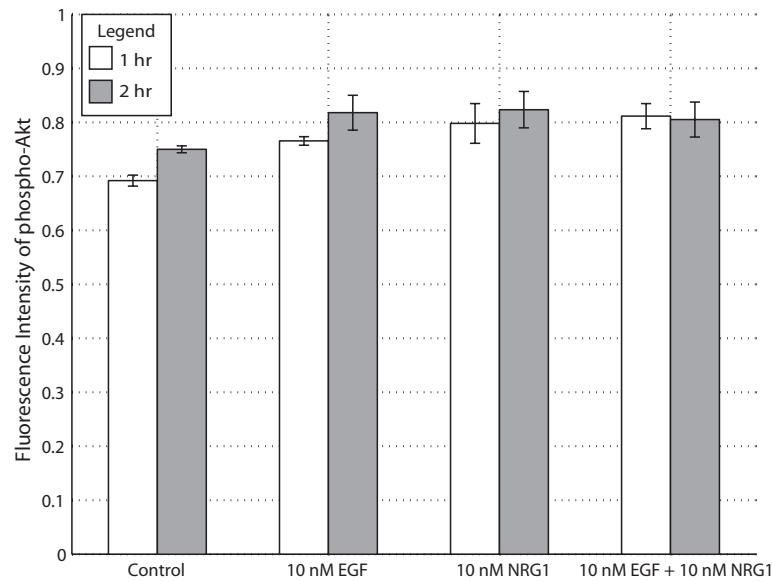


Figure A.4: Response of phospho-Akt to high concentration growth factor treatments.

Table A.2: p -values for phospho-Akt. Intensity levels detected for phospho-Akt in each treated, antibody-stained sample were compared to intensity levels detected in untreated, antibody-stained samples with a two-sample Student's t -test.

Treatment	p -values for phospho-Akt	
	1 hour	2 hours
1 nM EGF	0.052	0.023
1 nM NRG1	0.004	0.228
1 nM EGF + 1 nM NRG1	0.117	0.044
10 nM EGF	0.005	0.166
10 nM NRG1	0.093	0.157
10 nM EGF + 10 nM NRG1	0.081	0.227

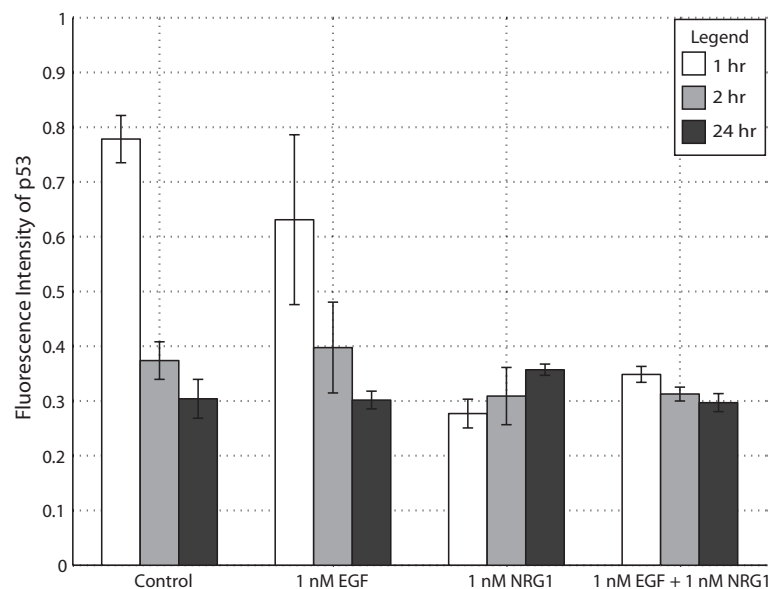


Figure A.5: Response of p53 to low concentration growth factor treatments.

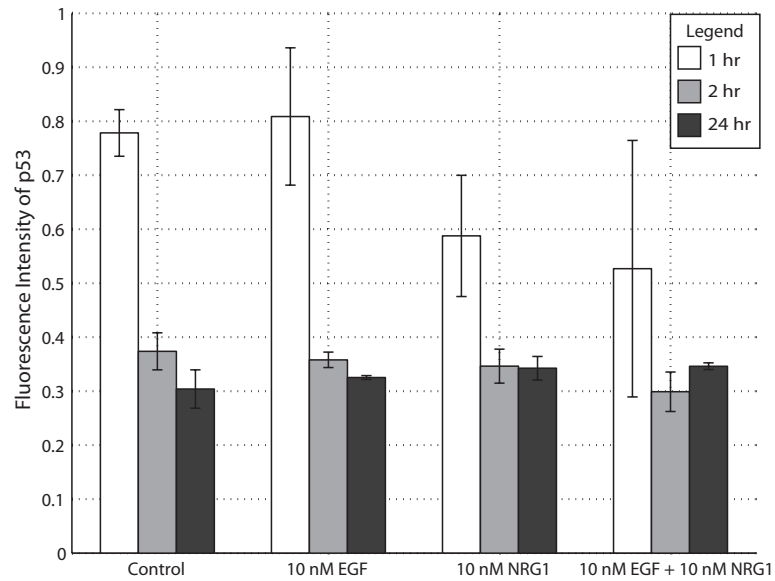


Figure A.6: Response of p53 to high concentration growth factor treatments.

Table A.3: p -values for p53. Intensity levels detected for p53 in each treated, antibody-stained sample were compared to intensity levels detected in untreated, antibody-stained samples with a two-sample Student's t -test.

Treatment	p -values for p53		
	1 hour	2 hours	24 hours
1 nM EGF	0.445	0.810	0.956
1 nM NRG1	0.001	0.367	0.270
1 nM EGF + 1 nM NRG1	0.005	0.209	0.868
10 nM EGF	0.838	0.702	0.611
10 nM NRG1	0.225	0.587	0.418
10 nM EGF + 10 nM NRG1	0.401	0.209	0.356

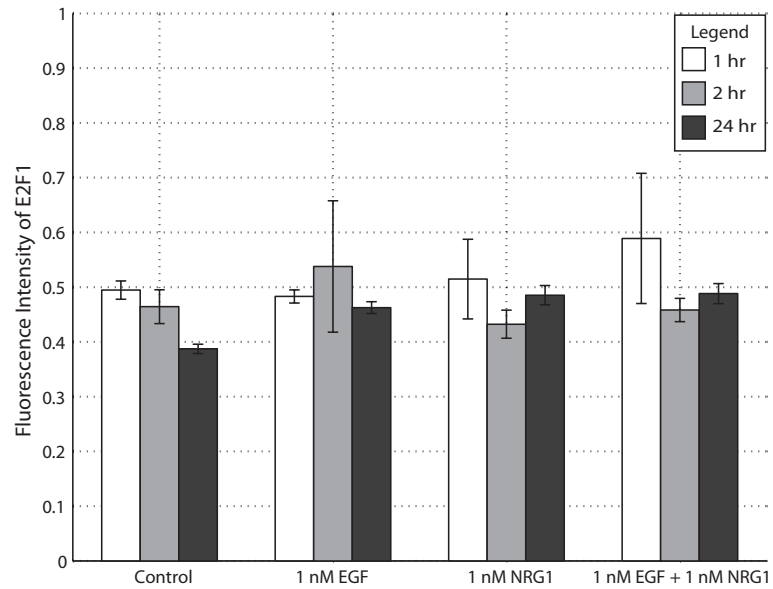


Figure A.7: Response of E2F1 to low concentration growth factor treatments.

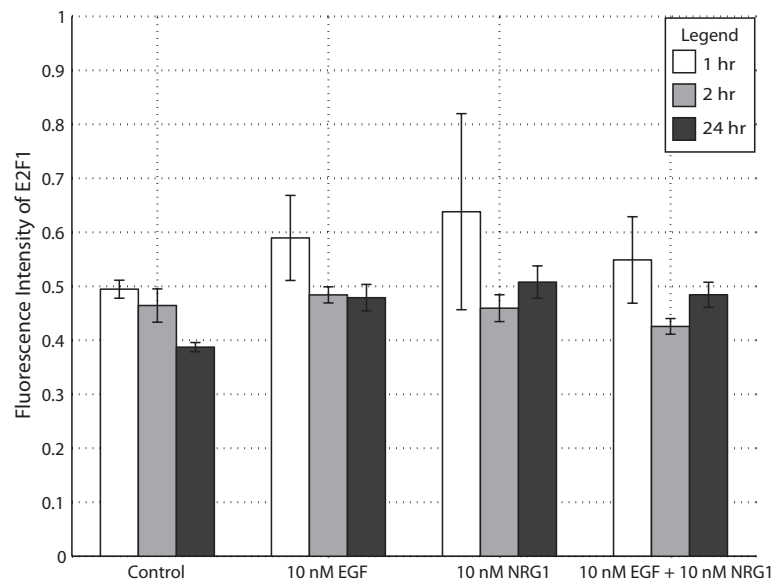


Figure A.8: Response of E2F1 to high concentration growth factor treatments.

Table A.4: p -values for E2F1. Intensity levels detected for E2F1 in each treated, antibody-stained sample were compared to intensity levels detected in untreated, antibody-stained samples with a two-sample Student's t -test.

Treatment	p -values for E2F1		
	1 hour	2 hours	24 hours
1 nM EGF	0.603	0.607	0.006
1 nM NRG1	0.810	0.472	0.016
1 nM EGF + 1 nM NRG1	0.511	0.879	0.070
10 nM EGF	0.351	0.606	0.051
10 nM NRG1	0.512	0.906	0.048
10 nM EGF + 10 nM NRG1	0.571	0.343	0.115

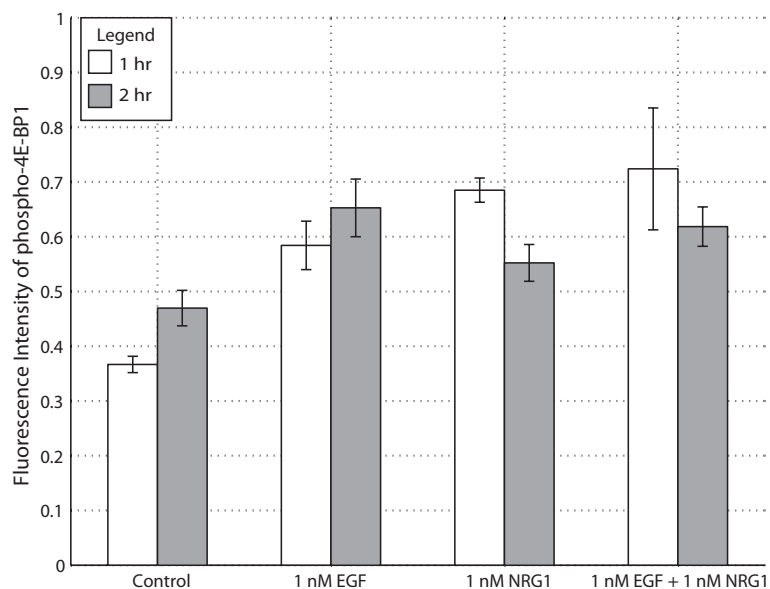


Figure A.9: Response of phospho-4E-BP1 to low concentration growth factor treatments.

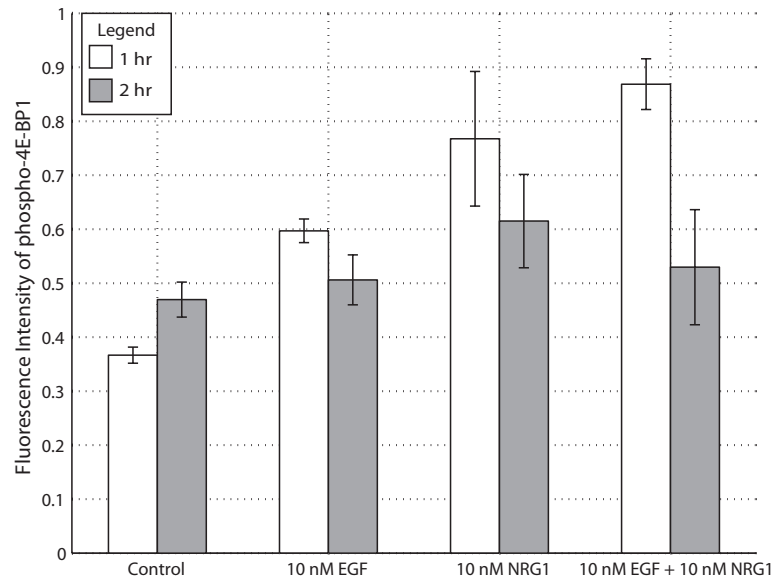


Figure A.10: Response of phospho-4E-BP1 to high concentration growth factor treatments.

Table A.5: p -values for phospho-4E-BP1. Intensity levels detected for phospho-4E-BP1 in each treated, antibody-stained sample were compared to intensity levels detected in untreated, antibody-stained samples with a two-sample Student's t -test.

Treatment	p -values for phospho-4E-BP1	
	1 hour	2 hours
1 nM EGF	0.028	0.052
1 nM NRG1	5.79E-04	0.150
1 nM EGF + 1 nM NRG1	0.082	0.037
10 nM EGF	0.001	0.556
10 nM NRG1	0.082	0.228
10 nM EGF + 10 nM NRG1	0.040	0.635

A.2 Comparison of fluorescence intensity between unstained and stained samples

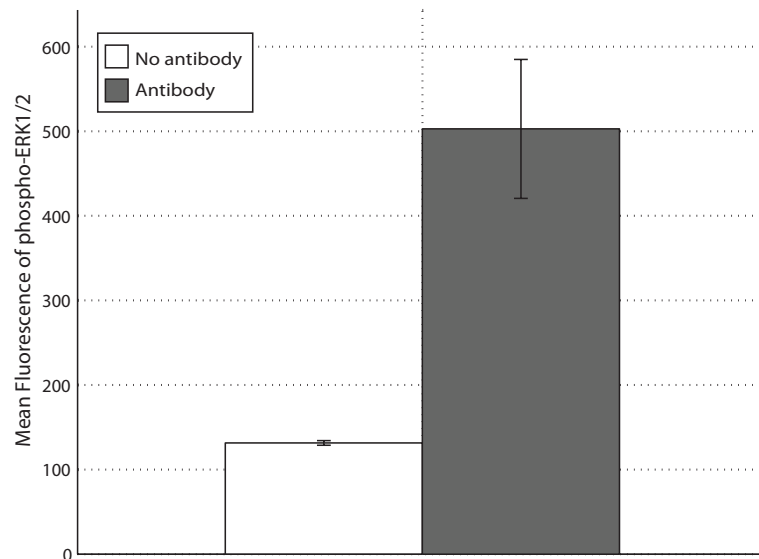


Figure A.11: Comparison of detected fluorescence for phospho-ERK1/2 between unstained and stained samples. Values across all time points were averaged and plotted with standard error. p -values listed in Table A.6.

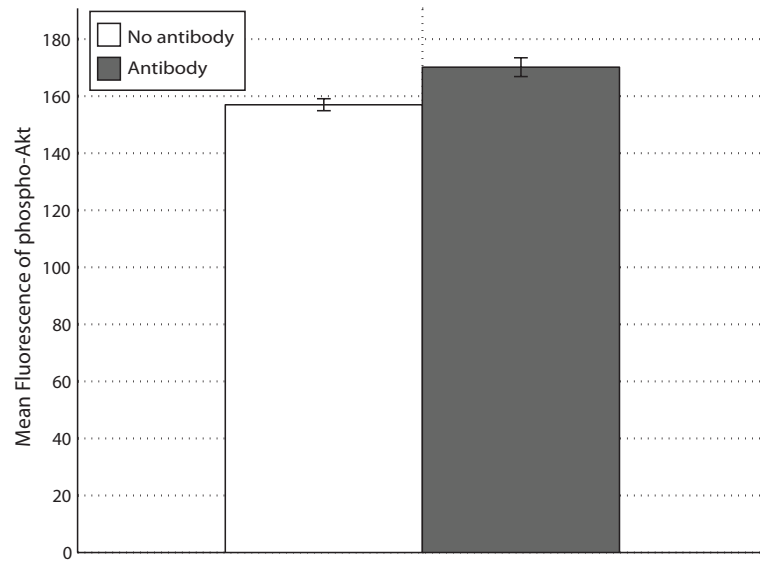


Figure A.12: Comparison of detected fluorescence for phospho-Akt between unstained and stained samples. Values across all time points were averaged and plotted with standard error. p -values listed in Table A.6.

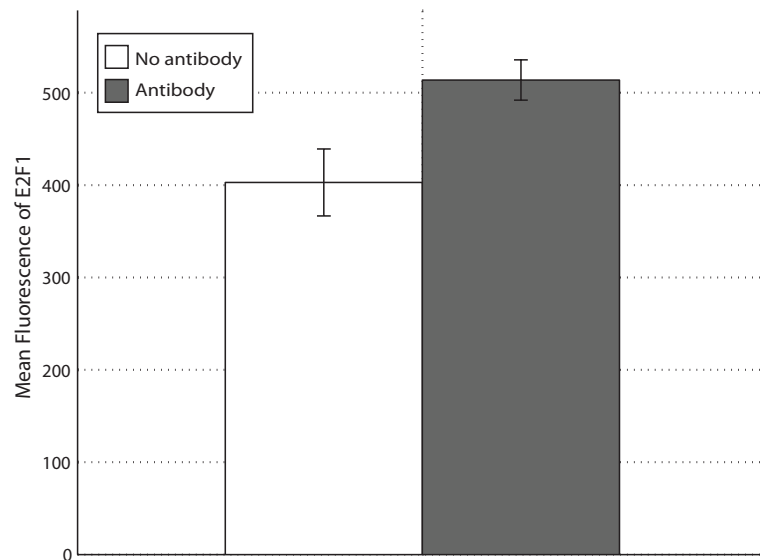


Figure A.13: Comparison of detected fluorescence for p53 between unstained and stained samples. Values across all time points were averaged and plotted with standard error. p -values listed in Table A.6.

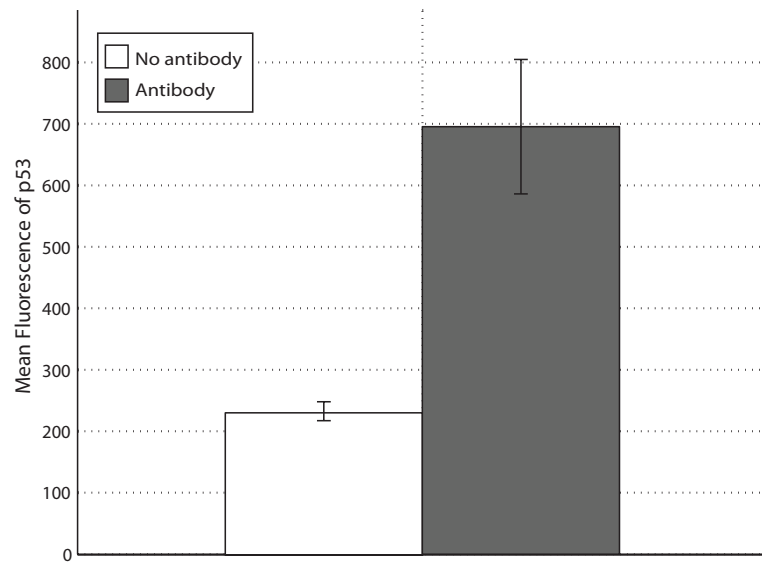


Figure A.14: Comparison of detected fluorescence for E2F1 between un-stained and stained samples. Values across all time points were averaged and plotted with standard error. p -values listed in Table A.6.

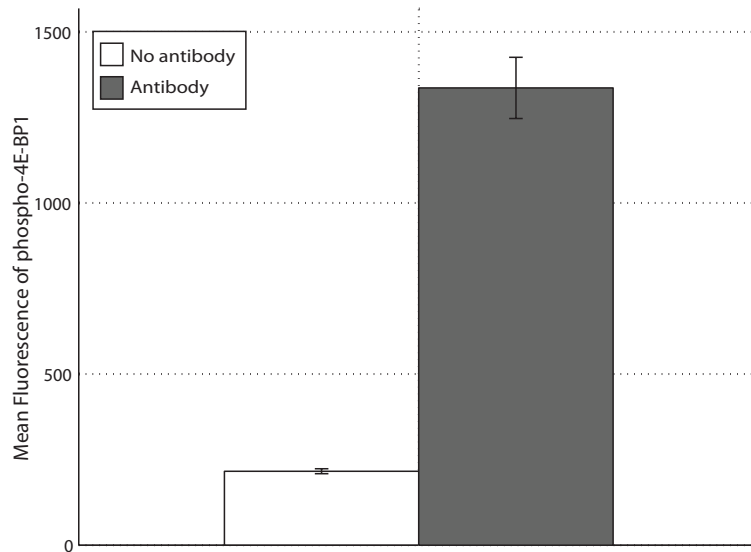


Figure A.15: Comparison of detected fluorescence for phospho-4E-BP1 between unstained and stained samples. Values across all time points were averaged and plotted with standard error. p -values listed in Table A.6.

Table A.6: p -values from two-sample Student's t -test between unstained and stained samples. Values across all time points were grouped together and simultaneously analyzed in the t -test.

Target	p -value
phospho-ERK1/2	1.94E-03
phospho-Akt	9.22E-03
E2F1	0.020
p53	0.002
phospho-4E-BP1	5.39E-05

A.3 Statistical significance of combination treatments

Table A.7: p -values from two-sample Student's t -test between the result due to a combination treatment ($\Delta_{EGF+NRG1}$) and the sum of a marker's response to just EGF and just NRG1 ($\Delta_{EGF} + \Delta_{NRG1}$).

Time	Concentration	p53	p-ERK1/2	E2F1	p-4E-BP1	p-Akt
1 hr	1 nM	0.012	0.559	0.724	0.123	0.109
	10 nM	0.372	0.079	0.092	0.077	0.076
2 hr	1 nM	0.351	0.023	0.241	0.027	1.0E-4
	10 nM	0.245	0.255	0.019	0.188	0.045
24 hr	1 nM	0.053	4.61E-4	0.046	–	–
	10 nM	0.104	0.607	0.018	–	–

APPENDIX B
NOMENCLATURE TABLE

Table B.1: Nomenclature reference index

Model reference [†]	Full name	Abbreviation
AKT1	Protein kinase B	Akt
AREG	Amphiregulin	AREG
BTC	Betacellulin	BTC
CCNA1	Cyclin A	CycA
CCNB1	Cyclin B	CycB
CCND1	Cyclin D	CycD
CCNE1	Cyclin E	CycE
CDC2	Cyclin dependent kinase 1	Cdk1
CDC25A	M-phase inducer phosphatase 1	Cdc25A
CDC25C	M-phase inducer phosphatase 3	Cdc25C
CDK2	Cyclin dependent kinase 2	Cdk2
CDK4	Cyclin dependent kinase 4	Cdk4
CDK6	Cyclin dependent kinase 6	Cdk6
CDKN1A	Cyclin dependent kinase inhibitor 1; p21; Waf1; Cip1	p21
CDKN1B	Cyclin-dependent kinase inhibitor 1B; p27; Cip2; Kip1	p27
cEx	Cellular exporter	cEx
CHEK1	Chk1 checkpoint homolog	Chk1
DAG	Diacylglycerol	DAG
E2F1	E2F1 transcription factor	E2F1

Continued on next page...

Table B.1 (Continued)

Model reference [†]	Full name	Abbreviation
EGF	Epidermal growth factor	EGF
EGFR	Epidermal growth factor receptor	EGFR
EIF4E	Eukaryotic translation initiation factor 4E	EIF4E
EIF4EBP1	Eukaryotic translation initiation factor 4E- binding protein 1	4E-BP1
ELK1	ETS-like gene 1	ELK
ERBB2	Epidermal growth factor receptor 2	HER2
ERBB3	Epidermal growth factor receptor 3	ErbB3
ERBB4	Epidermal growth factor receptor 4	ErbB4
EREG	Epiregulin	EREG
ETS1	E-twenty-six transcription factor	ETS1
FOS	c-Fos	Fos
GAP1m	Ras GTPase activating protein	GAP
GRB2	Growth factor receptor binding protein 2	Grb2
GSK3B	Glycogen synthase kinase 3b	GSK
HBEGF	Heparin-binding epidermal growth factor	HBEGF
IP3	Inositol 1,4,5-triphosphate	IP3
JUN	c-Jun	Jun
KRAS	c-Kirsten-ras protein	Ras
Lap	Lapatinib	Lap
MAP2K1	Mitogen-activated protein kinase/ERK kinase	MEK
MAPK1	Extracellular-signal-regulated kinase	ERK

Continued on next page...

Table B.1 (Continued)

Model reference [†]	Full name	Abbreviation
MAX	Myc -associated factor X	MAX
MTOR	Mammalian target of rapamycin	mTOR
MXD1	MAX dimerization protein 1	MAD
MYC	c-Myc	Myc
nEx	Nuclear exporter	nEx
nIm	Nuclear importer	nIm
NRG1	Neuregulin 1	NRG1
NRG2	Neuregulin 2	NRG2
NRG3	Neuregulin 3	NRG3
NRG4	Neuregulin 4	NRG4
Pase	Phosphatase	Pase
PDK1	Phosphoinositide-dependent kinase-1	PDK
PIK3CA	Phosphoinositide 3-kinase	PI3K
PIP2	Phosphatidylinositol 4,5-bisphosphate	PIP2
PIP3	Phosphatidylinositol 3,4,5-trisphosphate	PIP3
PLA2G4A	Cytosol phospholipase A2	PLA2
PLCG2	Phospholipase C, gamma 2	PLC
PLK1	Polo-like kinase 1	PLK
PPP1R3A	Protein phosphatase 1 regulatory subunit 3A	PP1
PPP2R5A	Protein phosphatase 2, regulatory subunit B, alpha	PP2
PPP5C	Protein phosphatase 5, catalytic subunit	PP5

Continued on next page...

Table B.1 (Continued)

Model reference [†]	Full name	Abbreviation
PRKCA	Protein kinase C, alpha	PKC
PTEN	Phosphatase and tensin homolog	PTEN
R40S	40S ribosomal subunit	40S
R60S	60S ribosomal subunit	60S
RAF1	Raf-1 protein kinase	Raf
Rap	Rapamycin	Rap
RB1	Retinoblastoma protein	Rb
RHEB	Ras homolog enriched in brain	Rheb
RNAp	RNA polymerase I	RNAp
RPS6KB1	Ribosomal protein S6 kinase	p70
SHC4	Src homology 2 domain containing	Shc
SOS1	Son of sevenless homolog 1	Sos
SP1	Specificity protein 1	Sp1
SP3	Specificity protein 3	Sp3
SRC	Sarcoma; c-Src	Src
SRF	Serum response factor	Srf
STAT3	Signal transducer and activator of tran- scription 3	STAT3
STAT5B	Signal transducer and activator of tran- scription 5B	STAT5B
TGFA	Transforming growth factor alpha	TGFa
TP53	Tumor protein 53	p53
TSC1	Tuberous sclerosis; hamartin	TCS1

Continued on next page...

Table B.1 (Continued)

Model reference [†]	Full name	Abbreviation
TSC2	Tuberous sclerosis; tuberin	TCS2
Wort	Wortmannin	Wort
YWHAB	tyrosine 3-monooxygenase/tryptophan 5-monooxygenase activation protein, beta polypeptide	14-3-3

[†]Also gene reference where applicable

BIBLIOGRAPHY

- [1] M. Alimandi, A. Romano, M. C. Curia, R. Muraro, P. Fedi, S. A. Aaronson, P. P. Di Fiore, and M. H. Kraus. Cooperative signaling of *erbB3* and *erbB2* in neoplastic transformation and human mammary carcinomas. *Oncogene*, 10(9):1813–1821, May 1995.
- [2] J. Baselga, D. Tripathy, J. Mendelsohn, S. Baughman, C. C. Benz, L. Dantis, N. T. Sklarin, A. D. Seidman, C. A. Hudis, J. Moore, P. P. Rosen, T. Twaddell, I. C. Henderson, and L. Norton. Phase ii study of weekly intravenous recombinant humanized anti-p185*her2* monoclonal antibody in patients with *her2/neu*-overexpressing metastatic breast cancer. *J Clin Oncol*, 14(3):737–744, Mar 1996.
- [3] M. Bébien, S. Salinas, C. Becamel, V. Richard, L. Linares, and R. A. Hipkind. Immediate-early gene induction by the stresses anisomycin and arsenite in human osteosarcoma cells involves *mapk* cascade signaling to *elk-1*, *creb* and *srf*. *Oncogene*, 22(12):1836–1847, Mar 2003.
- [4] L. Björnström and M. Sjöberg. Mechanisms of estrogen receptor signaling: convergence of genomic and nongenomic actions on target genes. *Mol Endocrinol*, 19(4):833–842, Apr 2005.
- [5] S. W. Blain and J. Massagu. Breast cancer banishes p27 from nucleus. *Nat Med*, 8(10):1076–1078, Oct 2002.
- [6] I. Blomberg and I. Hoffmann. Ectopic expression of *cdc25a* accelerates the *g(1)/s* transition and leads to premature activation of cyclin e- and cyclin a-dependent kinases. *Mol Cell Biol*, 19(9):6183–6194, Sep 1999.
- [7] F. A. Brightman and D. A. Fell. Differential feedback regulation of the *mapk* cascade underlies the quantitative differences in *egf* and *ngf* signalling in *pc12* cells. *FEBS Lett*, 482(3):169–174, Oct 2000.
- [8] A. Brunet, G. Pags, and J. Pouyssgur. Growth factor-stimulated *map* kinase induces rapid retrophosphorylation and inhibition of *map* kinase kinase (*mek1*). *FEBS Lett*, 346(2-3):299–303, Jun 1994.
- [9] D. V. Bulavin, Y. Higashimoto, Z. N. Demidenko, S. M., P. Graves, C. Phillips, H. Zhao, S. A. Moody, E. Appella, H. Piwnica-Worms, and A. J. Fornace. Dual phosphorylation controls *cdc25* phosphatases and mitotic entry. *Nat Cell Biol*, 5(6):545–551, Jun 2003.

- [10] S. Chandarlapaty, A. Sawai, M. Scaltriti, V. Rodrik-Outmezguine, O. Grbovic-Huezo, V. Serra, P. K. Majumder, J. Baselga, and N. Rosen. Akt inhibition relieves feedback suppression of receptor tyrosine kinase expression and activity. *Cancer Cell*, 19(1):58–71, Jan 2011.
- [11] W. W. Chen, B. Schoeberl, P. J. Jasper, Mario Niepel, U. B. Nielsen, D. A. Lauffenburger, and P. K. Sorger. Input-output behavior of erbb signaling pathways as revealed by a mass action model trained against dynamic data. *Mol Syst Biol*, 5:239, 2009.
- [12] M. Cheng, P. Olivier, J. A. Diehl, M. Fero, M. F. Roussel, J. M. Roberts, and C. J. Sherr. The p21(cip1) and p27(kip1) cdk ‘inhibitors’ are essential activators of cyclin d-dependent kinases in murine fibroblasts. *EMBO J*, 18(6):1571–1583, Mar 1999.
- [13] M. Cheng, V. Sexl, C. J. Sherr, and M. F. Roussel. Assembly of cyclin d-dependent kinase and titration of p27kip1 regulated by mitogen-activated protein kinase kinase (mek1). *Proc Natl Acad Sci U S A*, 95(3):1091–1096, Feb 1998.
- [14] C. Chou, D. Lee, H. Sun, L. Li, C. Lin, W. Huang, J. Hsu, H. Kuo, H. Yamaguchi, Y. Wang, M. Liu, H. Wu, P. Liao, C. Yen, and M. Hung. The suppression of mad1 by akt-mediated phosphorylation activates mad1 target genes transcription. *Mol Carcinog*, 48(11):1048–1058, Nov 2009.
- [15] I. Chu, J. Sun, A. Arnaout, H. Kahn, W. Hanna, S. Narod, P. Sun, C. Tan, L. Hengst, and J. Slingerland. p27 phosphorylation by src regulates inhibition of cyclin e-cdk2. *Cell*, 128(2):281–294, Jan 2007.
- [16] J. Chung, E. Uchida, T. C. Grammer, and J. Blenis. Stat3 serine phosphorylation by erk-dependent and -independent pathways negatively modulates its tyrosine phosphorylation. *Mol Cell Biol*, 17(11):6508–6516, Nov 1997.
- [17] L. Connell-Crowley, J. W. Harper, and D. W. Goodrich. Cyclin d1/cdk4 regulates retinoblastoma protein-mediated cell cycle arrest by site-specific phosphorylation. *Mol Biol Cell*, 8(2):287–301, Feb 1997.
- [18] O. Coqueret. New roles for p21 and p27 cell-cycle inhibitors: a function for each cell compartment? *Trends Cell Biol*, 13(2):65–70, Feb 2003.
- [19] P. Fojas de Borja, N. K. Collins, P. Du, J. Azizkhan-Cliford, and M. Mudryj. Cyclin a-cdk phosphorylates sp1 and enhances sp1-mediated transcription. *EMBO J*, 20(20):5737–5747, Oct 2001.

- [20] M. Dohadwala, E. F. da Cruz e Silva, F. L. Hall, R. T. Williams, D. A. Carbonaro-Hall, A. C. Nairn, P. Greengard, and N. Berndt. Phosphorylation and inactivation of protein phosphatase 1 by cyclin-dependent kinases. *Proc Natl Acad Sci U S A*, 91(14):6408–6412, July 1994.
- [21] M. Donzelli and G. F. Draetta. Regulating mammalian checkpoints through cdc25 inactivation. *EMBO Rep*, 4(7):671–677, Jul 2003.
- [22] J. Downward. Targeting ras signalling pathways in cancer therapy. *Nat Rev Cancer*, 3(1):11–22, Jan 2003.
- [23] J. W. Eckstein. Cdc25 protein phosphatase: regulation and its role in cancer. *Gene Ther Mol Biol*, 1:707–711, Mar 1998.
- [24] C.M. Fonseca and P.J. Fleming. Genetic algorithms for multiobjective optimization: Formulation, discussion and generalization. *Genetic Algorithms: Proceedings of the fifth international conference on genetic algorithms.*, 423:416–423, 1993.
- [25] K. G. Gadkar, F. J. Doyle, T. J. Crowley, and J. D. Varner. Cybernetic model predictive control of a continuous bioreactor with cell recycle. *Biotechnol Prog*, 19(5):1487–1497, 2003.
- [26] T. M. Gottlieb, J. F. M. Leal, R. Seger, Y. Taya, and M. Oren. Cross-talk between akt, p53 and mdm2: possible implications for the regulation of apoptosis. *Oncogene*, 21(8):1299–1303, Feb 2002.
- [27] D. Graus-Porta, R. R. Beerli, J. M. Daly, and N. E. Hynes. ErbB-2, the preferred heterodimerization partner of all erbB receptors, is a mediator of lateral signaling. *EMBO J*, 16(7):1647–1655, Apr 1997.
- [28] S. Gupta, A. Seth, and R. J. Davis. Transactivation of gene expression by myc is inhibited by mutation at the phosphorylation sites thr-58 and ser-62. *Proc Natl Acad Sci U S A*, 90(8):3216–3220, Apr 1993.
- [29] P. M. Guy, J. V. Platko, L. C. Cantley, R. A. Cerione, and K. L. Carraway. Insect cell-expressed p180erbB3 possesses an impaired tyrosine kinase activity. *Proc Natl Acad Sci U S A*, 91(17):8132–8136, Aug 1994.
- [30] C. Jane Hanson, Martin D Bootman, and H. Llewelyn Roderick. Cell signalling: Ip3 receptors channel calcium into cell death. *Curr Biol*, 14(21):R933–R935, Nov 2004.

- [31] J. W. Harper, S. J. Elledge, K. Keyomarsi, B. Dynlacht, L. H. Tsai, P. Zhang, S. Dobrowolski, C. Bai, L. Connell-Crowley, and E. Swindell. Inhibition of cyclin-dependent kinases by p21. *Mol Biol Cell*, 6(4):387–400, Apr 1995.
- [32] Y. Haupt, R. Maya, A. Kazaz, and M. Oren. Mdm2 promotes the rapid degradation of p53. *Nature*, 387(6630):296–299, May 1997.
- [33] H. Hayashi, Y. Tsuchiya, K. Nakayama, T. Satoh, and E. Nishida. Down-regulation of the pi3-kinase/akt pathway by erk map kinase in growth factor signaling. *Genes Cells*, 13(9):941–947, Sep 2008.
- [34] B. T. Hennessy, D. L. Smith, P. T. Ram, Y. Lu, and G. B. Mills. Exploiting the pi3k/akt pathway for cancer drug discovery. *Nat Rev Drug Discov*, 4(12):988–1004, Dec 2005.
- [35] S. W. Hiebert, S. P. Chellappan, J. M. Horowitz, and J. R. Nevins. The interaction of rb with e2f coincides with an inhibition of the transcriptional activity of e2f. *Genes Dev*, 6(2):177–185, Feb 1992.
- [36] A. C. Hindmarsh, P. N. Brown, K. E. Grant, S. L. Lee, R. Serban, D. E. Shumaker, and C. S. Woodward. Sundials: Suite of nonlinear and differential/algebraic equation solvers. *ACM Transactions on Mathematical Software*, 31(3):363–396, 2005.
- [37] I. Hoffmann, P. R. Clarke, M. J. Marcote, E. Karsenti, and G. Draetta. Phosphorylation and activation of human cdc25-c by cdc2–cyclin b and its involvement in the self-amplification of mpf at mitosis. *EMBO J*, 12(1):53–63, Jan 1993.
- [38] I. Hoffmann, G. Draetta, and E. Karsenti. Activation of the phosphatase activity of human cdc25a by a cdk2-cyclin e dependent phosphorylation at the g1/s transition. *EMBO J*, 13(18):4302–4310, Sep 1994.
- [39] R. Huang, J. Wu, Y. Fan, and E. D. Adamson. Uv activates growth factor receptors via reactive oxygen intermediates. *J Cell Biol*, 133(1):211–220, Apr 1996.
- [40] L. Hui, Y. Zheng, Y. Yan, J. Bargonetti, and D. A. Foster. Mutant p53 in mda-mb-231 breast cancer cells is stabilized by elevated phospholipase d activity and contributes to survival signals generated by phospholipase d. *Oncogene*, 25(55):7305–7310, Nov 2006.

- [41] R. Janknecht, W. H. Ernst, V. Pingoud, and A. Nordheim. Activation of ternary complex factor elk-1 by map kinases. *EMBO J*, 12(13):5097–5104, Dec 1993.
- [42] M. Jaumot and J. F. Hancock. Protein phosphatases 1 and 2a promote raf-1 activation by regulating 14-3-3 interactions. *Oncogene*, 20(30):3949–3958, Jul 2001.
- [43] A. Jemal, F. Bray, M. M. Center, J. Ferlay, E. Ward, and D. Forman. Global cancer statistics. *CA Cancer J Clin*, 61(2):69–90, 2011.
- [44] S. Jones, X. Zhang, D. W. Parsons, J. C. Lin, R. J. Leary, P. Angenendt, P. Mankoo, H. Carter, H. Kamiyama, A. Jimeno, S. Hong, B. Fu, M. Lin, E. S. Calhoun, M. Kamiyama, K. Walter, T. Nikolskaya, Y. Nikolsky, J. Hartigan, D. R. Smith, M. Hidalgo, S. D. Leach, A. P. Klein, E. M. Jaffee, M. Goggins, A. Maitra, C. Iacobuzio-Donahue, J. R. Eshleman, S. E. Kern, R. H. Hruban, R. Karchin, N. Papadopoulos, G. Parmigiani, B. Vogelstein, V. E. Velculescu, and K. W. Kinzler. Core signaling pathways in human pancreatic cancers revealed by global genomic analyses. *Science*, 321(5897):1801–1806, Sep 2008.
- [45] G. Karypis and V. Kumar. Multilevel k-way hypergraph partitioning. In *Proc. 36th Design Automation Conf*, pages 343–348, 1999.
- [46] J. Kato, H. Matsushime, S. W. Hiebert, M. E. Ewen, and C. J. Sherr. Direct binding of cyclin d to the retinoblastoma gene product (prb) and prb phosphorylation by the cyclin d-dependent kinase cdk4. *Genes Dev*, 7(3):331–342, Mar 1993.
- [47] B. N. Kholodenko, O. V. Demin, G. Moehren, and J. B. Hoek. Quantification of short term signaling by the epidermal growth factor receptor. *J Biol Chem*, 274(42):30169–30181, Oct 1999.
- [48] M. Kitagawa, H. Higashi, H. K. Jung, I. Suzuki-Takahashi, M. Ikeda, K. Tamai, J. Kato, K. Segawa, E. Yoshida, S. Nishimura, and Y. Taya. The consensus motif for phosphorylation by cyclin d1-cdk4 is different from that for phosphorylation by cyclin a/e-cdk2. *EMBO J*, 15(24):7060–7069, Dec 1996.
- [49] W. Kolch, G. Heidecker, G. Kochs, R. Hummel, H. Vahidi, H. Mischak, G. Finkenzeller, D. Marm, and U. R. Rapp. Protein kinase c alpha activates raf-1 by direct phosphorylation. *Nature*, 364(6434):249–252, Jul 1993.

- [50] L. Lin, M. Wartmann, A. Y. Lin, J. L. Knopf, A. Seth, and R. J. Davis. cpla2 is phosphorylated and activated by map kinase. *Cell*, 72(2):269–278, Jan 1993.
- [51] R. Linding, L. J. Jensen, G. J. Ostheimer, M. A. T. M. van Vugt, C. Jrgensen, I. M. Miron, F. Diella, K. Colwill, L. Taylor, K. Elder, P. Metalnikov, V. Nguyen, A. Pasculescu, J. Jin, J. G. Park, L. D. Samson, J. R. Woodgett, R. B. Russell, P. Bork, M. B. Yaffe, and T. Pawson. Systematic discovery of in vivo phosphorylation networks. *Cell*, 129(7):1415–1426, Jun 2007. NetworkIn.
- [52] C. W. Liu, R. H. Wang, M. Dohadwala, A. H. Schnthal, E. Villa-Moruzzi, and N. Berndt. Inhibitory phosphorylation of pp1alpha catalytic subunit during the g(1)/s transition. *J Biol Chem*, 274(41):29470–29475, Oct 1999.
- [53] B. Margolis and E. Y. Skolnik. Activation of ras by receptor tyrosine kinases. *J Am Soc Nephrol*, 5(6):1288–1299, Dec 1994.
- [54] K. L. Maughan, M. A. Lutterbie, and P. S. Ham. Treatment of breast cancer. *Am Fam Physician*, 81(11):1339–1346, Jun 2010.
- [55] D. Medina. The mammary gland: a unique organ for the study of development and tumorigenesis. *J Mammary Gland Biol Neoplasia*, 1(1):5–19, Jan 1996.
- [56] J. Milanini-Mongiat, J. Pouyssgur, and G. Pags. Identification of two sp1 phosphorylation sites for p42/p44 mitogen-activated protein kinases: their implication in vascular endothelial growth factor gene transcription. *J Biol Chem*, 277(23):20631–20639, Jun 2002.
- [57] P. Monje, M. J. Marinissen, and J. S. Gutkind. Phosphorylation of the carboxyl-terminal transactivation domain of c-fos by extracellular signal-regulated kinase mediates the transcriptional activation of ap-1 and cellular transformation induced by platelet-derived growth factor. *Mol Cell Biol*, 23(19):7030–7043, Oct 2003.
- [58] A. Montagnoli, F. Fiore, E. Eytan, A. C. Carrano, G. F. Draetta, A. Hershko, and M. Pagano. Ubiquitination of p27 is regulated by cdk-dependent phosphorylation and trimeric complex formation. *Genes Dev*, 13(9):1181–1189, May 1999.
- [59] D. O. Morgan. Cyclin-dependent kinases: engines, clocks, and microprocessors. *Annu Rev Cell Dev Biol*, 13:261–291, 1997.

- [60] S. Nayak, J. K. Siddiqui, and J. D. Varner. Modelling and analysis of an ensemble of eukaryotic translation initiation models. *IET Syst Biol*, 5(1):2, Jan 2011.
- [61] I. Nilsson and I. Hoffmann. Cell cycle regulation by the cdc25 phosphatase family. *Prog Cell Cycle Res*, 4:107–114, 2000.
- [62] M. Osaki, M. Oshimura, and H. Ito. Pi3k-akt pathway: its functions and alterations in human cancer. *Apoptosis*, 9(6):667–676, Nov 2004.
- [63] E. Perdiguero and A. R. Nebreda. Regulation of cdc25c activity during the meiotic g2/m transition. *Cell Cycle*, 3(6):733–737, Jun 2004.
- [64] O. Perisic, S. Fong, D. E. Lynch, M. Bycroft, and R. L. Williams. Crystal structure of a calcium-phospholipid binding domain from cytosolic phospholipase a2. *J Biol Chem*, 273(3):1596–1604, Jan 1998.
- [65] T. J. Pircher, H. Petersen, J. A. Gustafsson, and L. A. Haldosn. Extracellular signal-regulated kinase (erk) interacts with signal transducer and activator of transcription (stat) 5a. *Mol Endocrinol*, 13(4):555–565, Apr 1999.
- [66] F. Puntoni and E. Villa-Moruzzi. Phosphorylation of protein phosphatase-1 isoforms by cdc2-cyclin b in vitro. *Mol Cell Biochem*, 171(1-2):115–120, Jun 1997.
- [67] Y. W. Qian, E. Erikson, F. E. Taieb, and J. L. Maller. The polo-like kinase plx1 is required for activation of the phosphatase cdc25c and cyclin b-cdc2 in xenopus oocytes. *Mol Biol Cell*, 12(6):1791–1799, Jun 2001.
- [68] Z. Qu, J. N. Weiss, and W. R. MacLellan. Regulation of the mammalian cell cycle: a model of the g1-to-s transition. *Am J Physiol Cell Physiol*, 284(2):C349–C364, Feb 2003.
- [69] K. M. Quesnelle, A. L. Boehm, and J. R. Grandis. Stat-mediated egfr signaling in cancer. *J Cell Biochem*, 102(2):311–319, Oct 2007.
- [70] K. S. Ravichandran. Signaling via shc family adapter proteins. *Oncogene*, 20(44):6322–6330, Oct 2001.
- [71] M. J. Rebecchi and S. N. Pentylala. Structure, function, and control of phosphoinositide-specific phospholipase c. *Physiol Rev*, 80(4):1291–1335, Oct 2000.

- [72] A. K. Roshak, E. A. Capper, C. Imburgia, J. Fornwald, G. Scott, and L. A. Marshall. The human polo-like kinase, plk, regulates cdc2/cyclin b through phosphorylation and activation of the cdc25c phosphatase. *Cell Signal*, 12(6):405–411, Jun 2000.
- [73] P. Saha, Q. Eichbaum, E. D. Silberman, B. J. Mayer, and A. Dutta. p21cip1 and cdc25a: competition between an inhibitor and an activator of cyclin-dependent kinases. *Mol Cell Biol*, 17(8):4338–4345, Aug 1997.
- [74] A. Samanta, C. M. LeVea, W. C. Dougall, X. Qian, and M. I. Greene. Ligand and p185c-neu density govern receptor interactions and tyrosine kinase activation. *Proc Natl Acad Sci U S A*, 91(5):1711–1715, Mar 1994.
- [75] Y. Sanchez, C. Wong, R. S. Thoma, R. Richman, Z. Wu, H. Piwnicka-Worms, and S. J. Elledge. Conservation of the chk1 checkpoint pathway in mammals: linkage of dna damage to cdk regulation through cdc25. *Science*, 277(5331):1497–1501, Sep 1997.
- [76] F. Schmitt. Her2+ breast cancer: how to evaluate? *Adv Ther*, 26 Suppl 1:S1–S8, Jul 2009.
- [77] B. Schoeberl, C. Eichler-Jonsson, E. D. Gilles, and G. Mller. Computational modeling of the dynamics of the map kinase cascade activated by surface and internalized egf receptors. *Nat Biotechnol*, 20(4):370–375, Apr 2002.
- [78] W. X. Schulze, L. D., and M. Mann. Phosphotyrosine interactome of the erbb-receptor kinase family. *Mol Syst Biol*, 1:2005.0008, 2005.
- [79] R. Sears, F. Nuckolls, E. Haura, Y. Taya, K. Tamai, and J. R. Nevins. Multiple ras-dependent phosphorylation pathways regulate myc protein stability. *Genes Dev*, 14(19):2501–2514, Oct 2000.
- [80] R. Seger and E. G. Krebs. The mapk signaling cascade. *FASEB J*, 9(9):726–735, Jun 1995.
- [81] C. J. Sherr and F. McCormick. The rb and p53 pathways in cancer. *Cancer Cell*, 2(2):103–112, Aug 2002.
- [82] T. Shinomura, Y. Asaoka, M. Oka, K. Yoshida, and Y. Nishizuka. Synergistic action of diacylglycerol and unsaturated fatty acid for protein kinase c activation: its possible implications. *Proc Natl Acad Sci U S A*, 88(12):5149–5153, Jun 1991.

- [83] D. Silvera, S. C. Formenti, and R. J. Schneider. Translational control in cancer. *Nat Rev Cancer*, 10(4):254–266, Apr 2010.
- [84] B. L. Smith, D. Chin, W. Maltzman, K. Crosby, G. N. Hortobagyi, and S. S. Bacus. The efficacy of herceptin therapies is influenced by the expression of other erbb receptors, their ligands and the activation of downstream signalling proteins. *Br J Cancer*, 91(6):1190–1194, Sep 2004.
- [85] S. O. Song, A. Chakrabarti, and J. D. Varner. Ensembles of signal transduction models using pareto optimal ensemble techniques (poets). *Biotechnol J*, 5(7):768–780, Jul 2010.
- [86] C. S. Sørensen, R. G. Syljusen, J. Falck, T. Schroeder, L. Rönstrand, K. K. Khanna, B. Zhou, J. Bartek, and J. Lukas. Chk1 regulates the s phase checkpoint by coupling the physiological turnover and ionizing radiation-induced accelerated proteolysis of cdc25a. *Cancer Cell*, 3(3):247–258, Mar 2003.
- [87] J. D. Varner. Large-scale prediction of phenotype: concept. *Biotechnol Bioeng*, 69(6):664–678, Sep 2000.
- [88] K. Vermeulen, D. R. Van Bockstaele, and Z. N. Berneman. The cell cycle: a review of regulation, deregulation and therapeutic targets in cancer. *Cell Prolif*, 36(3):131–149, Jun 2003.
- [89] Q. J. Wang. Pkd at the crossroads of dag and pkc signaling. *Trends Pharmacol Sci*, 27(6):317–323, Jun 2006.
- [90] R. Wang, G. He, M. Nelman-Gonzalez, C. I. L. Ashorn, G. E. Gallick, P. T. Stukenberg, M. W. Kirschner, and J. Kuang. Regulation of cdc25c by erk-map kinases during the g2/m transition. *Cell*, 128(6):1119–1132, Mar 2007.
- [91] M. Wartmann, P. Hofer, P. Turowski, A. R. Saltiel, and N. E. Hynes. Negative modulation of membrane localization of the raf-1 protein kinase by hyperphosphorylation. *J Biol Chem*, 272(7):3915–3923, Feb 1997.
- [92] C. R. Weinstein-Oppenheim, W. L. Blalock, L. S. Steelman, F. Chang, and J. A. McCubrey. The raf signal transduction cascade as a target for chemotherapeutic intervention in growth factor-responsive tumors. *Pharmacol Ther*, 88(3):229–279, Dec 2000.

- [93] B. S. Wiseman and Z. Werb. Stromal effects on mammary gland development and breast cancer. *Science*, 296(5570):1046–1049, May 2002.
- [94] K. W. Wood, C. Sarnecki, T. M. Roberts, and J. Blenis. ras mediates nerve growth factor receptor modulation of three signal-transducing protein kinases: Map kinase, raf-1, and rsk. *Cell*, 68(6):1041–1050, Mar 1992.
- [95] Y. Yarden and M. X. Sliwkowski. Untangling the erbb signalling network. *Nat Rev Mol Cell Biol*, 2(2):127–137, Feb 2001.
- [96] E. Yeh, M. Cunningham, H. Arnold, D. Chasse, T. Monteith, G. Ivaldi, W. C. Hahn, P. T. Stukenberg, S. Shenolikar, T. Uchida, C. M. Counter, J. R. Nevins, A. R. Means, and R. Sears. A signalling pathway controlling c-myc degradation that impacts oncogenic transformation of human cells. *Nat Cell Biol*, 6(4):308–318, Apr 2004.
- [97] J. Zhu, J. Blenis, and J. Yuan. Activation of pi3k/akt and mapk pathways regulates myc-mediated transcription by phosphorylating and promoting the degradation of mad1. *Proc Natl Acad Sci U S A*, 105(18):6584–6589, May 2008.